

The age of volcanic tuffs from the Upper Freshwater Molasse (North Alpine Foreland Basin) and their possible use for tephrostratigraphic correlations across Europe for the Middle Miocene

Alexander Rocholl¹  · Urs Schaltegger² · H. Albert Gilg³ · Jan Wijbrans⁴ · Madelaine Böhme^{5,6}

Received: 12 April 2016 / Accepted: 29 May 2017
© Springer-Verlag GmbH Germany 2017

Abstract The Middle Miocene Upper Freshwater Molasse sediments represent the last cycle of clastic sedimentation during the evolution of the North Alpine Foreland Basin. They are characterized by small-scale lateral and temporal facies changes that make intra-basin stratigraphic correlations at regional scale difficult. This study provides new U–Pb zircon ages as well as revised ⁴⁰Ar/³⁹Ar data of volcanic ash horizons in the Upper Freshwater Molasse sediments from southern Germany and Switzerland. In a first and preliminary attempt, we propose their possible correlation to other European tephra deposits. The U–Pb zircon data of one Swiss (Bischofszell) and seven southern German (Zahling, Hachelstuhel, Laimering, Unterneul, Krumbad, Ponholz) tuff horizons indicate eruption ages between roughly 13.0 and 15.5 Ma. The stratigraphic position of the Unterneul and Laimering tuffs, bracketing the ejecta of the Ries impact (Brockhorizon), suggests that the Ries impact occurred

between 14.93 and 15.00 Ma, thus assigning the event to the reversed chron C5Bn1r (15.032–14.870 Ma) which is in accordance with paleomagnetic evidence. We combine our data with published ages of tuff horizons from Italy, Switzerland, Bavaria, Styria, Hungary, and Romania to derive a preliminary tephrochronological scheme for the Middle Miocene in Central Europe in the age window from 13.2 to 15.5 Ma. The scheme is based on the current state of knowledge that the Carpathian–Pannonian volcanic field was the only area in the region producing explosive calc-alkaline felsic volcanism. This preliminary scheme will require verification by more high-quality ages complemented by isotopic, geochemical and paleomagnetic data.

Keywords Tephrochronology · Middle Miocene · Upper Freshwater Molasse · Ries impact · Bentonites

✉ Alexander Rocholl
rocholl@gfz-potsdam.de

¹ Helmholtz Centre Potsdam, German Research Centre for Geosciences (GFZ), Telegrafenberg 1, 14473 Potsdam, Germany

² Department of Earth Sciences, University of Geneva, rue des Maraichers 13, 1205 Geneva, Switzerland

³ Lehrstuhl für Ingenieurgeologie, Technische Universität München, Arcisstr. 21, 80333 Munich, Germany

⁴ Faculty of Earth and Life Sciences, VU University Amsterdam, De Boelelan 1085, 1081 HV Amsterdam, The Netherlands

⁵ Terrestrische Paläoklimatologie, Senckenberg Center for Human Evolution and Palaeoenvironment, HEP Tübingen, Sigwartstr. 10, 72076 Tübingen, Germany

⁶ Department of Geoscience, University of Tübingen, Sigwartstr. 10, 72076 Tübingen, Germany

Introduction

Establishing a stratigraphic sequence of the Northern Alpine Foreland Basin (NAFB, Molasse basin) and extending this sequence to other parts of Europe are challenging due to the mainly clastic nature of the sedimentary infill. The Molasse basin stretches for about 1000 km from Lake Geneva to the Vienna Basin (Fig. 1a), containing not only continental but also marine and brackish sediments deposited during the Oligocene and Miocene as a result of foreland flexure during the Alpine orogeny. The youngest sedimentary succession of the Molasse basin comprises the clastic, mainly fluvial to limnic sediments of the Middle Miocene Upper Freshwater Molasse (Obere Süßwassermolasse, in the German literature). Regional chronostratigraphic correlation relies on a very small database of isotope geochronological data, and as a result, the recently

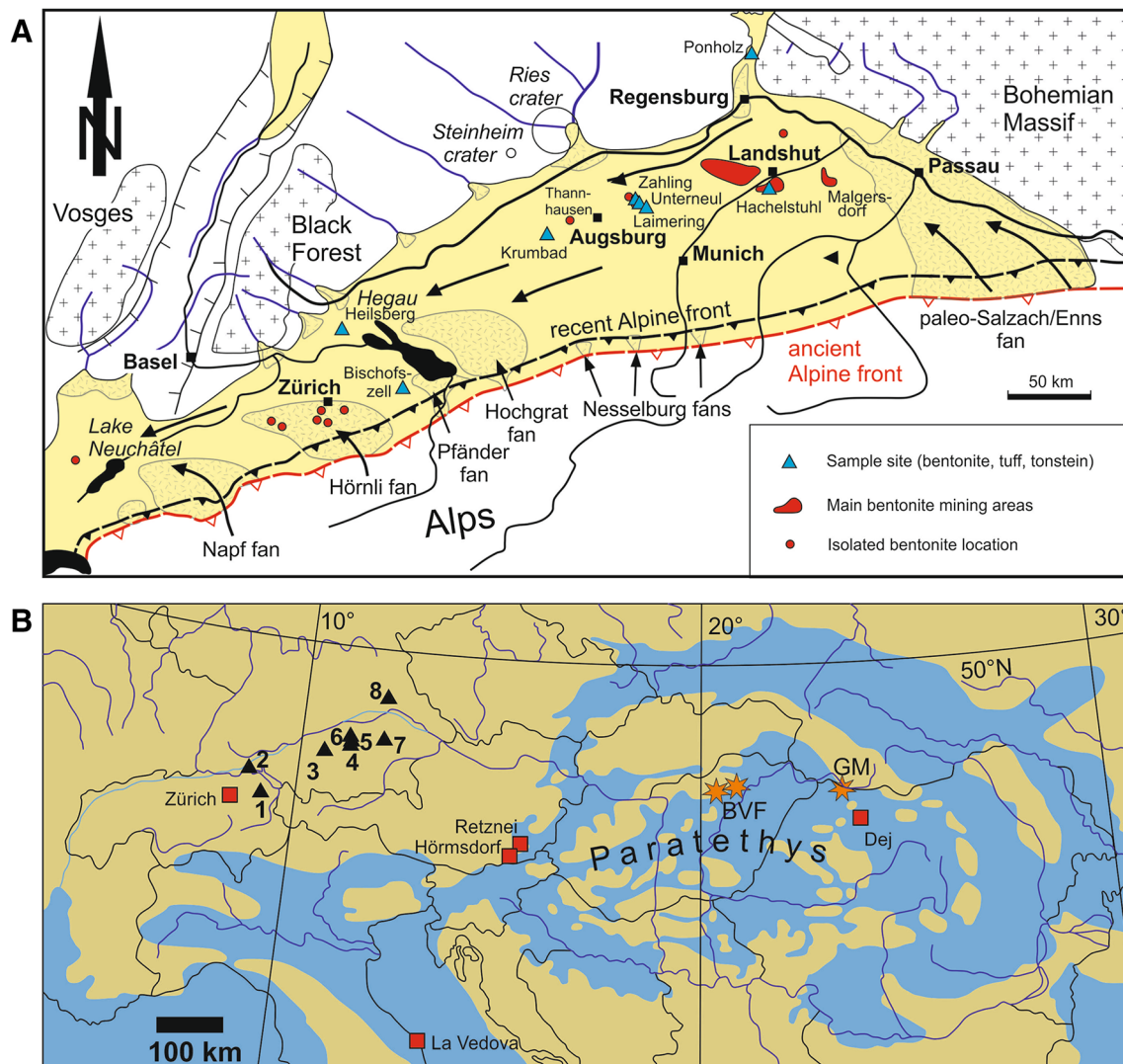


Fig. 1 **a** Schematic paleogeographic map of the North Alpine Foreland Basin (modified from Kuhlemann and Kempf 2002) with sample sites (blue triangles), bentonite occurrences (red), direction of Middle Miocene sediment transport (black arrows) and areas with prevailing erosion (white) and sedimentation (yellow). **b** Paleogeographic map of the Paratethys region during the late Early Badenian (ca. 15–14 Ma) modified from Rögl (1998) with the location of sampled

sites (black triangles), reference sites (red squares) and large calc-alkaline silicic volcanic centers (orange stars; according to Pécskay et al. 2006). BVF Bikkalja volcanic field, Hungary, GM Gutâi Mountains, Romania. 1 Bischofszell, 2 Heilsberg, 3 Krumbad, 4 Laimering, 5 Unterneul, 6 Zahling, 7 Hachelstuhl, 8 Ponholz

proposed correlations between the Swiss (Kälin and Kempf 2009) and the southern German molasse deposits (e.g., Bolliger 1994; Kälin and Kempf 2009; Aziz et al. 2008, 2010) are partially controversial (Reichenbacher et al. 2013).

This study provides new age constraints on several bentonite horizons derived from rhyolitic tuffs or tuffites that are intercalated in the German and Swiss Middle Miocene molasse sediments, respectively, as well as a recently discovered volcanogenic tonstein horizon in the largest tributary of the Molasse basin, the Paleo-Naab system. Weakly altered parts of the bentonite tuffs occasionally still

contain volcanic glass particles that had been dated using the $^{40}\text{Ar}/^{39}\text{Ar}$ method by Aziz et al. (2008, 2010). We present new ID-TIMS U–Pb zircon age determinations that are compared to revised $^{40}\text{Ar}/^{39}\text{Ar}$ ages reported in Aziz et al. (2008, 2010) using recently updated monitor age and decay constants (Kuiper et al. 2008; Min et al. 2000). The Molasse tuffs are thought to represent acidic ashes derived from the Carpathian–Pannonian region (Unger et al. 1990), which during the Mid-Miocene was part of the central Paratethys. This enables us to establish a preliminary tephrochronology model for Middle Miocene tuffs from western to eastern Central Europe.

Geological setting

The Molasse basin or NAFB forms a ca. 1000-km-long 10- to 200-km-broad depression along the Northern margin of the Alpine mountain belt, extending from Lake Geneva in the West to the eastern termination of the Alps near Vienna (Fig. 1a). The formation of the basin started during the mid-Cenozoic, mirroring the flexure of the European plate under the tectonic load of the evolving Alps (e.g., Home-wood et al. 1986; Schlunegger et al. 1997). Its sedimentary load ranges between a few tens of meters to more than 4 km in thickness and is subdivided on the basis of two long-term sedimentary cycles, representing two repetitive changes of clastic sedimentation from marine to continental conditions. The resulting sedimentary units comprise the Lower Marine/Freshwater Molasse (German: Untere Meeresmolasse/Untere Süßwassermolasse, UMM/USM) and the Upper Marine/Freshwater Molasse (German: Obere Meeresmolasse/Obere Süßwassermolasse, OMM/OSM). To avoid confusion, we will use here the abbreviations of the German terms which are most commonly used in literature.

The OSM represents the end of the second cycle of clastic sedimentation. With the beginning of the Middle Miocene at around 16.3 Ma, the marine Molasse Sea had totally retreated from the western part of the Molasse basin (Reichenbacher et al. 2013), leading to alluvial fan sedimentation in the southern rim of the basin and to predominantly fluvial sedimentation along the basin axis (Fig. 1a; Kuhlemann and Kempf 2002). Stratigraphic subdivision of OSM sediments may be obtained through bio-, litho-, and magnetostratigraphic methods, as well as by isotopic dating (e.g., Dehm 1951; Bolliger 1994; Heissig 1997; Kälin and Kempf 2009; Aziz et al. 2008, 2010; Gubler et al. 1992; Gubler 2009). This approach has to overcome ubiquitous lateral variability regarding transport direction, provenance, particle size, and lithofacies that are linked to complex basin geometry (e.g., Reichenbacher et al. 2013).

Despite the wealth of paleontological, paleoenvironmental, sedimentological, and, on a local scale, stratigraphic data (e.g., Aziz et al. 2010), precise intra-basin stratigraphic correlations at a larger scale are inconsistent and conflicting (e.g., Reichenbacher et al. 2013). Likewise, attempts to relate the sedimentary OSM record to the Astronomical Tuned Neogene Time Scale (ATNTS04; Lourens et al. 2004) are scant and insufficient, especially for the central part of the basin (e.g., Aziz et al. 2010; Reichenbacher et al. 2013).

The biostratigraphy is mainly based on small mammals (e.g., Bolliger 1992, 1994; Heissig 1997; Böhme et al. 2002; Aziz et al. 2008, 2010; Kälin and Kempf 2009; Prieto et al. 2009). The regional mammal stratigraphy in both the Swiss and German OSM have been independently

intercalibrated to magnetostratigraphic data and to the isotope geochronological data of intercalated bentonites and tuff layers (Gubler et al. 1992; Gubler 2009; Kälin and Kempf 2009; Aziz et al. 2008, 2010). The established stratigraphic framework appears internally consistent for each individual area but discloses significant and confusing inconsistencies when compared to each other. For example, biostratigraphically equivalent sediments would be up to 0.8 myr older in the German as compared to the Swiss Molasse basin (Reichenbacher et al. 2013).

In addition to the bentonites, the so-called Brockhorizont (or Blockhorizont in the Swiss part; Hofmann 1973) is another important stratigraphic time marker in the OSM of eastern Switzerland and southern Germany. The Brockhorizont represents a distal impact-generated ejecta layer resulting from the Ries meteorite impact at Nördlingen, southern Germany. It comprises angular blocks of Jurassic limestone, usually less than 20 cm in size, that were transported from the impact site for up to 180 km to the SE and SW (Reuter 1925; Stephan 1952; Böhme et al. 2002). It is significant to note that different stratigraphic studies applied different age estimates to the Ries event as a calibration anchor. The most recent compilation by Buchner et al. (2013) which considers $^{40}\text{Ar}/^{39}\text{Ar}$ ages obtained on various impact-generated glasses suggests an impact event occurred 14.74 ± 0.20 million years ago.

Middle Miocene bentonite, tuff, and tuffite beds occur as sporadic outcrops in the Molasse basin, stretching from a single outcrop near Lake Neuchâtel in the West (Hofmann 1958), several occurrences in the Zurich area (Pavoni and Schindler 1981; Gubler 2009) and a few north of St. Gallen (e.g., Bischofszell) in Switzerland, the Hegau (Hofmann 1956), through the central Molasse basin between Krumbach and Thannhausen (Harr 1976; Ulbig 1994; Scheuenpflug 1980), the Augsburg area (Fiest 1989; Aziz et al. 2010), to eastern Bavaria near Landshut (Vogt 1980; Unger and Niemeyer 1985a; Ulbig 1994, 1999; Köster and Gilg 2015; Gilg and Ulbig 2017) and Malgersdorf (Unger and Niemeyer 1985b). The bentonites consist mainly of montmorillonite formed from alteration of rhyolitic volcanic ash (Ulbig 1994; Aziz et al. 2008, 2010; Köster and Gilg 2015; Bauer et al. 2016).

In the Zurich area, the volcanic ash was deposited on the Hörnli fan (Fig. 1) and four stratigraphically distinct bentonite horizons are known (Pavoni and Schindler 1981; Gubler et al. 1992; Gubler 2009). The Ries ejecta layer, however, has not been found in the Zurich area. The thin bentonite beds occur about 65 m (Urdorf bentonite), 180 m (Küsnacht bentonite), 290 m (Auegstertal bentonite), and 310 m (Leimbach bentonite) above the south-dipping Meilener Kalk marker bed, a roughly 16 Ma old cemented arenite of the Hörnli fan (Bürgisser 1980; Gubler 2009). The beds have a thickness of less than 15 cm; glass

particles are not preserved, and non-volcanogenic detrital minerals are rare (Hofmann 1956; Hofmann et al. 1975; Pavoni and Schindler 1981).

This contrasts with many occurrences in the German part of the Molasse basin. Here, the bentonites occur as irregular lenses, that may reach a thickness of 0.5–3 m, occasionally even 8–10 m. At many locations, e.g., at Zahl- ing, E of Augsburg, or Strass near Mainburg, the central part of bentonite deposits often contain only slightly altered glass-rich indurated tuffite beds (“Harte Platte”). Most deposits are rich in non-volcanogenic, i.e., detrital minerals derived from the Molasse sediments, including illite/muscovite, chlorite, quartz, epidote, garnet and kyanite (Hofmann 1956; Harr 1976; Ulbig 1994). The most significant bentonite deposits occur in a 40-km-long and 10-km-wide NW–SE trending belt between Landshut and Mainburg (Vogt 1980; Unger and Niemeyer 1985a; Ulbig 1994, 1999; Gilg and Ulbig 2017) and further to the east near Malgersdorf (Unger and Niemeyer 1985b). Since their discovery in 1904, more than 200 individual deposits have been exploited in the Landshut–Mainburg area.

The geological environment and the petrographic characteristics suggests that the thick bentonite beds formed from reseedimented, accumulated ash in small oxbow lakes within a braided river system (Unger and Niemeyer 1985a, b; Ulbig 1999; Köster and Gilg 2015). In the Landshut area, the bentonites are aligned on a slightly south-dipping, uneven erosional surface (Ulbig 1999). Detailed mapping, however, revealed local elevation differences of up to 20 m which were interpreted either as representing a paleorelief (Ulbig 1999) or the presence of more than one bentonite horizon (Unger and Niemeyer 1985a; Unger et al. 1990). A third possible explanation may involve tectonic displacements (Gilg and Ulbig 2017). All bentonites in the Landshut area, are located few meters above the Brockhorizont (Ulbig 1999), while bentonite beds near Augsburg occur both above and below the Ries ejecta layer (Fiest 1989). The chemical composition of the volcanic ashes, from which the bentonites formed by alteration, was suggested as rhyolitic to dacitic based on analysis of bulk bentonite samples (Unger et al. 1990), while analyses of separated glass particles revealed exclusively rhyolitic compositions (Ulbig 1999; Aziz et al. 2008, 2010; Gilg 2005). On the basis of their trace and major element composition and age, the source of the volcanic ashes was attributed to the Carpathian-Pannonian province by Unger and Niemeyer (1985b). The paleogeographic map shown in Fig. 1b depicts the location of Early Badenian (ca. 14–15 Ma) eruption centers of calc-alkaline rhyolitic pyroclastic rocks in the central Paratethys region and shows the sites of investigated and correlated samples.

A distinct, few cm-thick kaolinitic tonstein (Weisse Lasse) occurs in the lignite-bearing refractory clay deposit

Rohrhof II near Ponholz, Bavaria (Kromer 1980; Viertel 1995; Gilg and Ulbig 2017; Fig. 2). The tonstein contrasts in composition with the montmorillonitic bentonites. It represents an altered tephra layer in coal-bearing sequences that is transformed to kaolinite due to the acidity of the aqueous environment (Bohor and Triplehorn 1993). The deposit occurs within the Miocene fluvial Paleo-Naab system which represents the largest northern preserved tributary to the OSM at the western border of the Bohemian Massif (Wappenschmidt 1936).

Samples

The samples in this study derive from the western (Bischofszell, Heilsberg), central (Krumbad, Laimering, Unterneul, Zahl- ing) and eastern (Hachelstuh) part of the Molasse basin and the Paleo-Naab tributary near Ponholz (Fig. 1a). Mineralogical and chemical data are presented in Ulbig (1994) and Aziz et al. (2008, 2010). With the exception of Ponholz, the samples had been taken 20 years earlier in small quantities, and only little material was left behind for zircon separation. Meanwhile, almost all of the sampled pits in Germany have been backfilled and cannot be accessed again.

The Bischofszell samples originate from the 0.5-m-thick basal bentonite layer underlying a 1.7-m-thick tuffite at Rengishalde (−47.489307°N, 9.210068°E, 520 m a.s.l.) NW of St. Gallen (Hofmann 1956). The unusual thick deposit occurs at the NE rim of the Hörnli fan. It is probably related to the bentonite occurrence of Mollen near Waldkirch (Fischer 1988) that occurs about 100 m above the Ries impact layer (Reichenbacher et al. 1998).



Fig. 2 Weisse Lasse tonstein, a white kaolinized volcanic ash horizon, in lignite seam III of the Middle Miocene Braunkohlentertiär in the Rohrhof II open pit at Ponholz

A 1.3-m-thick bentonite layer (Basisbentonit) within the Oberer Haldenhofmergel (Hofmann 1956; Sawatzki and Schreiner 1991; Doppler et al. 2005) occurs at the eastern side of the Heilsberg (47.750077°N, 8.785201°E, 520 m a.s.l.) near Gottmadingen in the Hegau area (Hofmann 1956; Harr 1976; Schreiner 2008). It contains abundant, up to 150- μ m-sized fragments of pumiceous volcanic glass of rhyolitic composition that survived the securitization process.

The Krumbad bentonite near Krumbach, west of Augsburg (48.244415°N, 10.389827°E, 550 m a.s.l.), has a thickness of about 6 m, and also contains abundant particles of pumiceous rhyolitic glass (Scheuenpflug 1980; Ulbig 1994). It is located within the Fluviale Untere Serie (Ulbig 1994; Doppler 1989) below the Ries impact ejection layer (Brockhorizont) (Aziz et al. 2010).

At Zahling near Dasing, 12 km northeast of Augsburg, two distinct bentonite beds (Zahling-1 and Zahling-2) have been sampled. The 2-m-thick Zahling-1 bentonite (48.428761°N, 11.030712°E, 512 m a.s.l.) occurs only 5 m above the 7-m-thick glass-rich tuffite of Zahling-2 (48.427985°N, 11.034713°E, 505 m a.s.l.). The stratigraphic context has been described by Schmid (1995) and interpreted by Aziz et al. (2010) as an erosional unconformity, but may also be interpreted by tectonic displacement (Fig. 5). Zahling-1 bentonite is no longer accessible.

At Unterneul near Gallenbach, a 5-cm-thick tuff horizon occurs at 469 m a.s.l. directly below the Brockhorizont (Fig. 5). The outcrop situation is described in Fiest (1989) who place the (no longer accessible) profile (Horizonte von Unterneul) at the base of the composite section around Laimering/Gallenbach. In contrast to other volcanic ashes of this study, the Unterneul tuff is characterized by fining-upward grading of biotite phenocrysts (Fiest 1989) and common magnetite–ilmenite intergrowth (Ulbig 1994).

A 2-m-thick bentonite horizon was exposed in the brickyard Laimering (1 km NE of Laimering) between 493 and 495 m a.s.l. (Fiest 1989; Fig. 5). Stratigraphically, it belongs to the upper part of the Gallenbach Serie (Fiest 1989), about 20 m above the Ries impact layer.

The Hachelstuhl bentonite deposit (48.480273°N, 12.150056°E, 450 m a.s.l.) is considered as part of the so-called main bentonite horizon of the Mainburg–Landshut area, eastern Bavaria. It was one of the largest bentonite deposits south of Landshut reaching several meters in thickness and displaying an internal tuffite layer enriched in residual glass fragments (Ulbig 1999). The Hachelstuhl pit has been backfilled and can no longer be accessed.

The kaolinitic Weisse Lasse tonstein at the Rohrhof II pit near Ponholz (Fig. 2) occurs within the lignite seam III in the upper part of the lignite–clay unit (Braunkohlentertiär) (Kromer 1980; Viertel 1995; Gilg and Ulbig 2017).

A geological section through the lignite–clay successions at Rohrhof II is presented in Fig. 3 (Viertel 1995). The few cm-thick Weisse Lasse tonstein (49.189744°N, 12.084557°E, 381 m a.s.l.) contains residual sanidine, biotite, and magmatic quartz with melt inclusions and euhedral zircon, suggesting a rhyolitic protolith (Gilg and Ulbig 2017). The presence of the rodent *Anomalomys* minor in the lignite–clay unit indicates a Karpathian to Early Badenian age (Viertel 1995).

Methods

U–Pb age determinations

The U–Pb age determinations were carried using chemical abrasion, isotope dilution, thermal ionization mass spectrometry (CA-ID-TIMS) techniques that were the state of

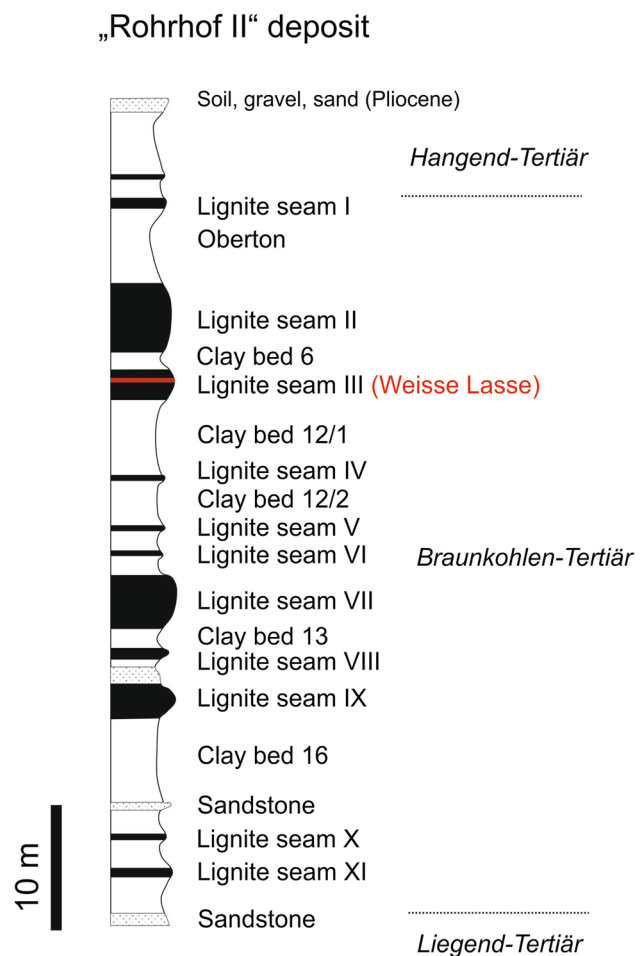


Fig. 3 Schematic geological section of the Rohrhof II pit with the position of the Weisse Lasse tonstein within a succession of intercalated clay and lignite beds (Viertel 1995)

the art in 2008 in the geochronology laboratory of University of Geneva.

Sample preparation: Chemical abrasion (Mattinson 2005) involved annealing of separated zircon grains of each sample in quartz crucibles at 900 °C for ca. 48 h. Zircons were subsequently transferred into 3-ml screw-top Savillex vials together with ca. 120 µl concentrated HF and 20 µl 7 N HNO₃ for the partial dissolution step. Savillex vials were arranged into a Teflon Parr™ vessel with 2 ml concentrated HF, and placed in an oven at 180 °C for 12–15 h. After partial dissolution, the leachate was pipetted out and the remaining zircons were rinsed in ultrapure water and then fluxed for several hours in 6 N HCl on a hot-plate at a temperature of ca. 80 °C. The acid solution was removed and the fractions were again rinsed several times in ultrapure water and acetone in an ultrasonic bath. Single zircons were selected, weighed and loaded for dissolution into pre-cleaned miniaturized Teflon vessels. After adding a mixed ²⁰⁵Pb–²³³U–²³⁵U spike (EARTHTIME, Condon et al. 2015) zircons were dissolved in 63 µl concentrated HF with a drop of 7 N HNO₃ at 206 °C for 6 days, evaporated and redissolved overnight in 36 µl 3 N HCl at 206 °C. Pb and U were separated by HCl-based anion exchange chromatography in ca. 40-µl micro-columns and dried down with 3 µl of 0.05 N H₃PO₄.

Mass spectrometry and blank: The isotopic analyses were performed on a TRITON mass spectrometer equipped with a MasCom secondary electron multiplier (SEM). Its linearity was calibrated using U500, Sr SRM987, and Pb SRM982 and SRM983 solutions. The mass fractionation of Pb was controlled by repeated SRM981 and SRM982 measurements (0.13 ± 0.02 1σ %/amu). The U mass fractionation for the same analyses was calculated using the ²³³U–²³⁵U ratio of the double-spike solution ($0.99464 \pm 0.01\%$, 1σ). Both lead and uranium were loaded with 1 µl of silica gel–phosphoric acid mixture (Gerstenberger and Haase 1997) on outgassed single refilaments. Pb isotopes were measured on the SEM, while U (as UO₂) isotopic measurements were made in static Faraday mode using high-sensitivity amplifiers equipped with 10¹² Ohm resistors, or, in case of very low-U samples, on the SEM. Isobaric interference of ²³³U¹⁸O¹⁶O on ²³⁵U¹⁶O¹⁶O was corrected using a ¹⁸O/¹⁶O ratio of 0.00205. All ²⁰⁶Pb/²³⁸U and ²⁰⁷Pb/²⁰⁶Pb ratios were corrected for initial disequilibrium in ²³⁰Th/²³⁸U using Th/U [magma] = 4 (Schärer 1984). All common Pb for the zircon analyses was attributed to procedural blank with the following isotopic composition: ²⁰⁶Pb/²⁰⁴Pb: 18.30 ± 0.70 , ²⁰⁷Pb/²⁰⁴Pb: 15.47 ± 1.03 , ²⁰⁸Pb/²⁰⁴Pb: 37.60 ± 0.98 (all 1σ percent error). U blanks are <0.1 pg and do not influence the degree of discordance at the age range of the studied samples, and therefore a value of $0.05 \text{ pg} \pm 50\%$ was used in all data reduction.

Data reduction, reporting ages and errors: The initial statistics was done using the TRIPOLI program (Bowring et al. 2011) followed by data reduction and age calculation using the YourLab spreadsheet with the algorithms of Schmitz and Schoene (2007). All data are reported in Table 1 with internal errors only (X error after Schoene et al. 2006), including counting statistics, uncertainties in correcting for mass discrimination, and the uncertainty in the common (blank) Pb composition. For mean ages, Y errors (including systematic errors such as tracer calibration) and Z errors (including decay constant uncertainties) have been added. The MSWD values of weighted mean from all samples are within the range of acceptable values at 95% confidence level and for $n-1$ degrees of freedom, defined by Wendt and Carl (1991); otherwise, the youngest date of a given sample was adopted. Accuracy and internal reproducibility of the U–Pb data was assessed by repeated analysis of chemically abraded R33 standard zircon (Black et al. 2004), measured at an average ²⁰⁶Pb/²³⁸U age of 419.08 ± 0.19 Ma ($n = 27$; MSWD = 0.70). The 100 Ma synthetic solution measured at that time with EARTHTIME ²⁰²Pb–²⁰⁵Pb–²³⁵U–²³⁸U tracer (Condon et al. 2008) and calculated using U–Pb_Redux software (Bowring et al. 2011; spike ET2535v3) yielded mean ²⁰⁶Pb/²³⁸U = 100.202 ± 0.018 Ma ($n = 19$, MSWD = 1.4).

⁴⁰Ar/³⁹Ar age determinations

In our initial study, we focused on ⁴⁰Ar/³⁹Ar dating of clean and optically unaltered pumiceous glass fragments sampled from the least altered, glass-rich parts of the bentonites. The dated pumice particles are described in Ulbig (1994). The highly vesicular glass shards display irregular angular to slightly rounded shapes, ranging in size mostly between 100 and 150 µm, rarely reaching 250 µm. Vesicle shapes vary from roundish to strongly stretched (fragments of tube pumice). Roundish vesicles have diameters between <1 and several tens of µm to elongated, while vesicles in tube pumice may extend across the complete pumice fragment. The obtained ⁴⁰Ar/³⁹Ar ages were published in Aziz et al. (2008, 2010). Here, we recalculate the published ⁴⁰Ar/³⁹Ar ages, which were based on the decay constants of Steiger and Jäger (1977; $\lambda_{\text{tot}} = 5.543 \times 10^{-10} \text{ a}^{-1}$) and on FCs monitor age of 28.02 ± 0.28 Ma (Renne et al. 1998). We follow the approach of Kuiper et al. (2008) in combining the recently and astronomically intercalibrated age estimate for the FCs monitor (Kuiper et al. 2008; 28.201 ± 0.046 Ma) with the decay constant of Min et al. (2000; $\lambda_{\text{tot}} = 5.463 \pm 0.214 \times 10^{-10} \text{ year}^{-1}$). This approach, which is also consistent with the EARTHTIME consensus, has shown to be the most successful in reproducing U/Pb zircon ages in young

Table 1 U–Th–Pb isotopic data

Sample ^a	Compositional parameters				Radiogenic isotope ratios				Isotopic ages (Ma)											
	Wt. mg ^b	U ppm ^c	Th/U ^d	Pb*/Pbc ^e	206Pb/204Pbf	207Pb/206Pbg	%2σ ^h 207Pb/235Ug	%2σ ^h 206Pb/238Ug	Corr. coef.	207Pb/206Pbi	±2σ ^h	207Pb/235Ui	±2σ ^h	206Pb/238Ui	±2σ ^h					
																Pb*/Pbc ^e	Pb ppm ^c			
Zahlinger-1																				
ZAH1/ z1	0.0009	521	0.30	9.21	0.13	7.34	27	0.0468	19.19	0.01336	19.89	0.002071	2.94	0.31	38.36	457.6	13.48	2.66	13.34	0.39
ZAH1/ z3	0.0003	562	0.95	8.28	0.19	2.08	30	0.0317	56.26	0.00985	58.21	0.002256	2.63	0.75	-995.55	1659.4	9.96	5.77	14.53	0.38
ZAH1/ z4	0.0007	436	0.50	6.90	0.16	4.15	29	0.0444	24.65	0.01333	25.77	0.002176	2.29	0.52	-87.75	602.3	13.44	3.44	14.01	0.32
ZAH1/ z5	0.0002	663	1.10	13.52	0.13	2.39	26	0.0310	85.61	0.00936	88.53	0.002188	3.89	0.76	-1056.63	2559.5	9.46	8.34	14.09	0.54
Bischofszell																				
Bs2b/z1	0.0007	902	0.44	9.67	0.26	5.38	34	0.0474	12.21	0.01405	12.77	0.002151	1.41	0.44	68.94	289.69	14.17	1.80	13.85	0.19
Bs2b/z2	0.0093	593	0.35	1.39	18.68	0.66	1186	0.0468	0.50	0.01446	0.54	0.002239	0.10	0.49	40.42	11.84	14.57	0.08	14.42	0.01
Bs2b/z3	0.0033	537	0.41	1.42	6.03	0.67	390	0.0465	1.39	0.01440	1.48	0.002243	0.12	0.69	25.98	33.30	14.51	0.21	14.45	0.02
Bs2b/z4	0.0040	672	0.55	1.73	10.49	0.60	640	0.0468	0.83	0.01445	0.89	0.002238	0.10	0.61	40.19	19.87	14.57	0.13	14.41	0.01
Bs2b/z5	0.0030	355	0.53	1.04	3.93	0.64	252	0.0476	2.30	0.01471	2.43	0.002242	0.27	0.53	77.66	54.50	14.82	0.36	14.44	0.04
Bs2b/z6	0.0010	675	0.50	2.43	1.83	0.86	128	0.0471	4.48	0.01457	4.73	0.002245	0.28	0.91	53.00	106.57	14.69	0.69	14.46	0.04
Hachelstuhl																				
Ha2a/z1	0.0014	440	0.66	1.73	1.73	0.89	117	0.0479	5.27	0.01517	5.56	0.002297	0.39	0.76	93.43	124.42	15.29	0.84	14.79	0.06
Ha2a/z2	0.0031	87	0.65	0.82	0.38	1.83	40	0.0543	19.70	0.01747	20.91	0.002335	1.31	0.93	381.62	441.70	17.58	3.64	15.03	0.20
Ha2a/z3	0.0029	72	0.61	1.35	0.18	3.31	29	0.0575	25.36	0.02037	26.95	0.002572	2.20	0.74	509.01	556.46	20.48	5.46	16.56	0.36
Ha2a/z5	0.0036	196	0.60	0.68	2.40	0.72	158	0.0484	4.06	0.01527	4.28	0.002290	0.36	0.63	117.18	95.41	15.39	0.65	14.75	0.05
Ha2a/z6	0.0047	102	0.58	0.41	1.60	0.73	111	0.0484	5.68	0.01533	6.00	0.002296	0.41	0.79	120.08	133.50	15.45	0.92	14.78	0.06
Zahlinger-2																				
ZAH2b/ z1	0.0010	1094	0.70	3.29	5.63	0.50	340	0.0467	1.64	0.01505	1.74	0.002338	0.14	0.72	32.70	39.22	15.16	0.26	15.05	0.02
ZAH2/ z1	0.0049	83	0.58	0.54	0.61	1.65	54	0.0476	13.61	0.01536	14.37	0.002339	0.99	0.77	80.97	322.33	15.48	2.21	15.06	0.15
ZAH2/ z2	0.0010	220	0.68	5.21	0.12	4.66	26	0.0380	45.09	0.01241	46.57	0.002366	3.35	0.47	-482.55	1192.11	12.52	5.80	15.24	0.51
ZAH2/ z5	0.0010	162	0.56	1.74	0.29	1.35	36	0.0424	31.57	0.01378	33.04	0.002359	1.93	0.78	-204.51	789.22	13.90	4.56	15.19	0.29
ZAH2/ z6	0.0002	1864	0.68	12.05	0.64	1.47	55	0.0500	12.70	0.01582	13.43	0.002296	0.98	0.76	193.42	294.43	15.93	2.12	14.78	0.14
ZAH2/ z3	0.0010	549	0.47	5.18	0.69	3.06	61	0.0474	6.94	0.02450	7.32	0.003750	0.58	0.68	68.82	164.78	24.58	1.78	24.13	0.14
ZAH2/ z4	0.0002	2413	0.49	196.11	26.32	1.44	1602	0.0563	0.25	0.58362	0.30	0.075147	0.08	0.68	465.27	5.62	466.78	1.13	467.09	0.37
Krumbad																				
Bat1/z1	0.0010	331	0.61	1.79	0.87	0.96	69	0.0493	9.37	0.01596	10.01	0.002346	0.69	0.94	163.75	218.45	16.08	1.60	15.11	0.10
Bat1/z2	0.0010	110	0.68	1.06	0.39	0.76	40	0.0573	20.56	0.01879	22.08	0.002380	1.68	0.91	501.51	451.67	18.90	4.14	15.32	0.26

Table 1 (continued)

Sample ^a	Compositional parameters				Radiogenic isotope ratios				Isotopic ages (Ma)										
	U ppm ^c	Th/U ^d	Pb ppm ^e	Pb*/Pbc ^e (pg)	²⁰⁶ Pb/ ²⁰⁴ Pb ^f	²⁰⁷ Pb/ ²⁰⁶ Pb ^g	%2 σ^h ²⁰⁷ Pb/ ²³⁵ U ^g	%2 σ^h ²⁰⁶ Pb/ ²³⁸ U ^g	%2 σ^h	Corr. coef.	²⁰⁷ Pb/ ²⁰⁶ Pb	$\pm 2 \sigma^h$ ²⁰⁷ Pb/ ²³⁵ U ⁱ	$\pm 2 \sigma^h$ ²⁰⁶ Pb/ ²³⁸ U ⁱ	$\pm 2 \sigma^h$					
Bat1/z3	0.0010	146	0.66	0.69	0.57	56	0.0603	19.44	0.01946	20.12	0.002339	1.13	0.62	615.69	418.93	19.57	3.90	15.06	0.17
Laimering																			
Lai1a/1	0.0012	1475	0.68	4.25	6.88	412	0.0472	1.36	0.01508	1.44	0.002318	0.14	0.59	58.76	32.42	15.20	0.22	14.93	0.02
Lai1a/2	0.0051	1532	0.81	4.07	44.29	2474	0.0465	0.48	0.01488	0.50	0.002319	0.14	0.32	26.03	11.40	15.00	0.07	14.93	0.02
Lai1a/6	0.0044	447	0.61	1.22	8.98	543	0.0465	1.13	0.01485	1.19	0.002317	0.13	0.51	22.83	26.99	14.97	0.18	14.92	0.02
Lai1a/4	0.0023	344	0.75	1.19	3.04	688	0.0480	3.00	0.01540	3.17	0.002326	0.21	0.82	100.49	70.67	15.52	0.49	14.98	0.03
Lai1a/3	0.0021	396	0.84	1.42	5.25	488	0.0470	1.92	0.01719	2.03	0.002654	0.18	0.61	47.71	45.88	17.31	0.35	17.09	0.03
Untemeul																			
L1a/1	0.0005	1666	0.57	5.43	3.06	67	0.0470	2.75	0.01509	2.91	0.002330	0.20	0.82	47.56	65.41	15.21	0.44	15.00	0.03
L1a/2	0.0005	1597	0.55	6.05	1.83	107	0.0475	4.53	0.01526	4.79	0.002330	0.32	0.84	73.53	107.29	15.37	0.73	15.00	0.05
L1a/3	0.0010	1002	0.52	3.35	2.74	90	0.0470	3.08	0.01524	3.26	0.002351	0.24	0.76	49.30	73.36	15.35	0.50	15.14	0.04
L1a/4	0.0010	295	0.54	1.36	1.14	63	0.0478	7.74	0.01536	8.19	0.002329	0.55	0.82	91.07	182.97	15.48	1.26	15.00	0.08
L1a/5	0.0003	1628	0.50	5.54	2.45	48	0.0473	3.48	0.01520	3.68	0.002330	0.26	0.81	65.14	82.64	15.32	0.56	15.01	0.04
Ponholz																			
WL1/z1	0.0020	850	0.68	2.93	2.95	148	0.0464	1.57	0.01521	1.68	0.002377	0.13	0.83	18.62	37.61	15.33	0.26	15.31	0.02
WL1/z2	0.0029	268	0.45	1.36	0.94	203	0.0474	3.46	0.01573	3.66	0.002409	0.39	0.54	67.52	82.14	15.85	0.58	15.51	0.06
WL1/z4	0.0024	501	0.50	2.04	1.53	193	0.0464	2.35	0.01526	2.49	0.002387	0.27	0.55	16.62	56.33	15.38	0.38	15.37	0.04
WL1/z5	0.0049	489	0.60	1.64	3.02	200	0.0461	1.10	0.01515	1.18	0.002382	0.14	0.63	5.23	26.41	15.27	0.18	15.34	0.02
WL1/z6	0.0024	295	0.56	1.48	1.02	176	0.0482	3.87	0.01593	4.09	0.002395	0.41	0.57	110.92	91.12	16.05	0.65	15.42	0.06

^az1, z2 etc. are labels for single zircon grains or fragments; all zircons annealed and chemically abraded after Mattinson (2005)

^bNominal fraction weights measured after chemical abrasion

^cNominal U and total Pb concentrations subject to uncertainty in weighting zircons

^dModel Th/U ratio calculated from radiogenic ²⁰⁸Pb/²⁰⁶Pb ratio and ²⁰⁷Pb/²³⁵U age

^ePb* and Pbc represent radiogenic and common Pb, respectively

^fMeasured ratio corrected for spike and fractionation only. Mass fractionation correction for Pb of 0.13 ± 0.02 (1-sigma, %/amu (atomic mass unit) was applied to all single-collector SEM measurements based on analyses of SRM 981 and SRM 982. Mass fractionation correction for U was done using the ²³⁵U/²³⁸U ratio of the EARTHTIME ²³⁵U–²³³U–²⁰⁵Pb tracer (Condon et al. 2015)

^gCorrected for fractionation, spike, and common Pb; all common Pb was assumed to be procedural blank: ²⁰⁶Pb/²⁰⁴Pb = 18.30 \pm 0.26%; ²⁰⁷Pb/²⁰⁴Pb = 15.47 \pm 0.32%; ²⁰⁸Pb/²⁰⁴Pb = 37.60 \pm 0.74% (all uncertainties 1-sigma). ²⁰⁶Pb/²³⁸U and ²⁰⁷Pb/²⁰⁶Pb ratios corrected for initial disequilibrium in ²³⁰Th/²³⁸U using Th/U [magma] = 4

^hErrors are 2-sigma, propagated using the algorithms of Schmitz and Schoene (2007) and Crowley et al. (2007)

ⁱCalculations are based on the decay constants of Jaffey et al. (1971). ²⁰⁶Pb/²³⁸U and ²⁰⁷Pb/²⁰⁶Pb ages corrected for initial disequilibrium in ²³⁰Th/²³⁸U using Th/U [magma] = 4

volcanic rocks (e.g., Channell et al. 2010; Phillips and Matchan 2013; Zeeden et al. 2014; Jicha et al. 2016). To allow comparison, we also applied the alternative constants and monitor age by Renne et al. (2011).

Results

The U–Pb ID-TIMS results for individual zircons are listed in Table 1 and presented in stratigraphic order as $^{206}\text{Pb}/^{238}\text{U}$ age-ranked distribution plots (Fig. 4). The mean $^{206}\text{Pb}/^{238}\text{U}$ ages range between 13.3 and 15.3 Ma. They are compiled in Table 2 and compared to the $^{40}\text{Ar}/^{39}\text{Ar}$ ages from Aziz et al. (2008, 2010) recalculated on the basis of two sets of recent estimates of decay constants (Min et al. 2000; Renne et al. 2011) and FCs monitor ages (Kuiper et al. 2008; Renne et al. 2011), respectively.

Five zircons from the Weisse Lasse tonstein (Ponholz) yielded a scatter of $^{206}\text{Pb}/^{238}\text{U}$ ages between 15.51 and 15.31 Ma, possibly reflecting prolonged residence time in the magma chamber. Since no mean age can be calculated, we may adopt the youngest $^{206}\text{Pb}/^{238}\text{U}$ age of 15.32 ± 0.02 Ma (2σ) as an approximate age of eruption and ash deposition, being aware that this youngest date may be biased by non-resolved post-crystallization loss of radiogenic Pb despite the chemical abrasion procedure.

Sample Krumbad provided a mean $^{206}\text{Pb}/^{238}\text{U}$ age of 15.120 ± 0.083 Ma (MSWD = 1.5; 2σ error) from three analyses. The elevated uncertainties are due to sub-microgram zircon sample weights, resulting in radiogenic Pb/common Pb ratios below unity.

Four zircons from the Unterneul bentonite define an age of $15.003 \pm 0.024/0.028/0.033$ Ma. A fourth zircon was dated at 15.14 ± 0.04 Ma, pointing to protracted residence time in the magma chamber.

The three youngest zircon crystals of the Laimering bentonite yielded a mean $^{206}\text{Pb}/^{238}\text{U}$ age of $14.925 \pm 0.012/0.019/0.025$ Ma. A fourth crystal at 14.98 ± 0.03 Ma is indicative of prolonged residence time, while a fifth crystal (17.09 ± 0.03 Ma) reflects a slight xenocrystic contribution.

Seven zircons of Zahling-2 tuff show a considerable age spectrum, ranging roughly between 15 and 470 Ma, clearly indicating the presence of xenocrystic zircon. Three analyses yielded an apparent age of 15.055 ± 0.021 Ma, with two further analyses from xenocrystic zircon at $^{206}\text{Pb}/^{238}\text{U}$ dates of 24.1 and 467 Ma (not plotted in Fig. 4). One significantly younger data point at 14.78 ± 0.14 Ma does not belong statistically to the same population. Since this youngest zircon date is in line with the post-Ries stratigraphic position, we adopt this latter age as an approximation for eruption and ash bed deposition.

The three youngest zircon grains from sample Hachelstuhl yielded a mean $^{206}\text{Pb}/^{238}\text{U}$ age of $14.772 \pm 0.032/0.035/0.038$ Ma (MSWD = 0.83), while two older grains with presumed inheritance of older Pb plot at $^{206}\text{Pb}/^{238}\text{U}$ dates of 15.03 and 16.55 Ma.

Five zircon grains analyzed from sample Bischofszell are statistically non-equivalent and yield scattered $^{206}\text{Pb}/^{238}\text{U}$ dates between 14.41 and 14.46 Ma. While two grains are slightly older, grains 2, 4, and 5 yield a precise mean $^{206}\text{Pb}/^{238}\text{U}$ age of $14.417 \pm 0.009/0.017/0.023$ Ma (MSWD = 0.84).

Four zircon analyses from Zahling-1 bentonite did not yield reproducible $^{206}\text{Pb}/^{238}\text{U}$ dates, with an older Pb component at least in grain 3. Adopting the same interpretation strategy as for the previous samples, we suggest a minimum age of 13.34 ± 0.39 Ma for the deposition of this tuff, based on the youngest zircon.

Average $^{40}\text{Ar}/^{39}\text{Ar}$ ages of glass fragments recalculated from Aziz et al. (2008, 2010; see above) are reported in Table 2 with $\pm 2\sigma$ analytical and standard intercalibration uncertainties. The data do not include the uncertainties of the chosen FCs monitor ages (0.16%, Kuiper et al. 2008; 0.13% Renne et al. 2011) and decay constants (3.9%, Min et al. 2000; 0.4% Renne et al. 2011). Note that the difference between ages calculated on the basis of the Kuiper/Min vs. Renne values is about 50 ka and thus insignificant with respect to the analytical error.

Discussion

The recalculated set of $^{40}\text{Ar}/^{39}\text{Ar}$ data by Aziz et al. (2008, 2010) and the new $^{206}\text{Pb}/^{238}\text{U}$ zircon ages disclose some surprising stratigraphic relationships within the OSM successions. The data open new questions with respect to the timing of some sedimentary units and the number of sedimentary OSM cycles. A major drawback of the new $^{206}\text{Pb}/^{238}\text{U}$ ages is the limited number of analyzed zircon grains due to the small rock volumes sampled 20 years ago.

$^{40}\text{Ar}/^{39}\text{Ar}$ vs. U–Pb ages: the recalculated $^{40}\text{Ar}/^{39}\text{Ar}$ ages of Aziz et al. (2008, 2010) presented in Table 2 exceed the published $^{40}\text{Ar}/^{39}\text{Ar}$ ages by some 90 ka or 0.6%. For comparison, we also list the ages recalculated using the alternative constants by Renne et al. (2011), which increases the published $^{40}\text{Ar}/^{39}\text{Ar}$ ages to even $>1\%$. Three tuffs have been dated with both the $^{40}\text{Ar}/^{39}\text{Ar}$ and U–Pb zircon methods, namely Hachelstuhl, Zahling-2 and Krumbad.

Within errors, the apparent $^{40}\text{Ar}/^{39}\text{Ar}$ ages are either identical (Hachelstuhl) or older (Krumbad, Zahling-2) than the respective ^{238}U – ^{206}Pb zircon ages. In the case of Zahling-2, however, $^{40}\text{Ar}/^{39}\text{Ar}$ ages exceed ^{238}U – ^{206}Pb ages by more than 1.4 million years. We explain this inconsistency

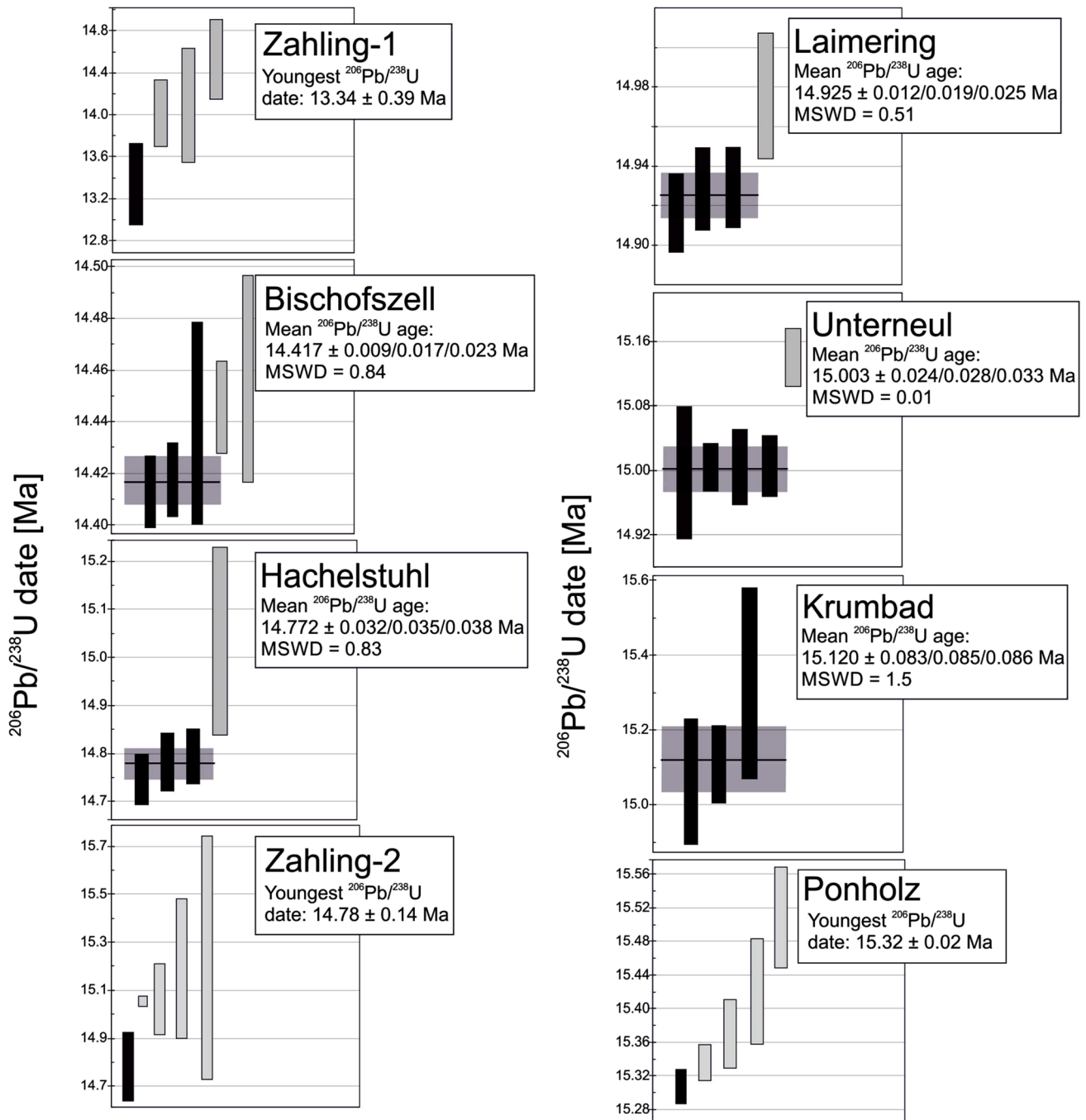


Fig. 4 $^{206}\text{Pb}/^{238}\text{U}$ single zircon ages of Middle Miocene tuff and bentonite beds from the Molasse basin and Paleo-Naab system, arranged in stratigraphic order and presented as $^{206}\text{Pb}/^{238}\text{U}$ age-ranked distribution plots. The data cover a total range of around 2 Ma and range

from pre- to post-Ries ages. Black columns indicate those data, which were used for determining the respective eruption ages, as explained under chapter results

between both chronometers by a decreased $^{40}\text{K}/^{40}\text{Ar}$ ratio due to disturbance of the K–Ar system. Possible scenarios include inherited argon as well as open system behavior of the fine-walled glass fragments during alteration and/or neutron irradiation. Disturbance by incorporation of excess argon has been suggested to explain the offset

between plateau and isochron ages in some of the Hachelstuhl and Heilsberg glasses (Aziz et al. 2008, 2010) but failed to explain the Zahling-2 data (Aziz et al. 2010). Preferred mobilization and loss of potassium over argon during alteration or weathering of rhyolitic pumice have been suggested by Cerling et al. (1985) to explain K–Ar ages of

Table 2 Single zircon $^{206}\text{Pb}/^{238}\text{U}$ and $^{40}\text{Ar}/^{39}\text{Ar}$ ages (glass, plagioclase) from OSM bentonites/tuffs and the Weisse Lasse tonstein at Ponholz

	$^{206}\text{Pb}/^{238}\text{U}$ (Ma)*	$^{40}\text{Ar}/^{39}\text{Ar}$ (Ma) Publ. ^a	$^{40}\text{Ar}/^{39}\text{Ar}$ (Ma) Recalc. ^b	$^{40}\text{Ar}/^{39}\text{Ar}$ (Ma) Recalc. ^c
Zahling-1	13.34 ± 0.39	–	–	–
Bischofszell	14.417 ± 0.009	–	–	–
Heilsberg (glass)	–	14.62 ± 0.31	14.71 ± 0.31	14.76 ± 0.31
Heilsberg (plag)	–	14.54 ± 0.14	14.63 ± 0.14	14.68 ± 0.14
Hachelstuhl	14.772 ± 0.032	14.55 ± 0.19	14.64 ± 0.19	14.69 ± 0.19
Zahling-2d	14.78 ± 0.14	16.10 ± 0.22	16.20 ± 0.22	16.26 ± 0.22
Laimering	14.925 ± 0.012	–	–	–
Unterneul	15.003 ± 0.024	–	–	–
Krumbad	15.120 ± 0.083	15.62 ± 0.37	15.72 ± 0.37	15.77 ± 0.10
Ponholz	15.32 ± 0.02	–	–	–

Errors refer to 2-sigma and do not include uncertainties of the decay constants and/or monitor ages. Samples are arranged in stratigraphic order

^aPublished $^{40}\text{Ar}-^{39}\text{Ar}$ ages from Aziz et al. (2008, 2010)

^bRecalculated $^{40}\text{Ar}-^{39}\text{Ar}$ ages based on recent estimates for the FCTs monitor age and the ^{40}K decay constant by Kuiper et al. (2008) and Min et al. (2000)

^cRecalculated ages based on the Renne et al. (2011) values

^dThe $^{40}\text{Ar}-^{39}\text{Ar}$ ages of Zahling-2 represent the mean of two total fusion and one step-heating analyses

pumice exceeding respective sanidine ages obtained by the $^{40}\text{Ar}/^{39}\text{Ar}$ method. Note that such a process was, explicitly ruled out for the Zahling-2 glasses on the basis of $^{39}\text{Ar}-^{37}\text{Ar}-^{36}\text{Ar}$ (K–Ca–Ar) systematics (Aziz et al. 2010). Recoil loss of ^{39}Ar during irradiation is a well-studied phenomenon. It becomes a significant problem especially when analyzing fine grained minerals (e.g., Jordan et al. 2007; Villa 1997) or vitreous materials (Morgan et al. 2009). Pumiceous material like the Zahling-2 glasses is characterized by extreme porosity and the highest surface-area-to-volume ratio known of any rock type (Brasier et al. 2011), making this material especially prone to recoil loss. For example, Karner et al. (1999) report on anomalous old ages of pumiceous tephra which they solely explain by this process. Recoil loss of ^{39}Ar therefore appears to us to be the most likely process to explain the anomalous old ages of the Zahling-2 glass fragments.

In summary, we consider the U–Pb zircon ages obtained on glasses as more reliable than the $^{40}\text{Ar}/^{39}\text{Ar}$ data which should only be interpreted as maximum ages. Thus, for our stratigraphic interpretation, we will consider exclusively the $^{40}\text{Ar}/^{39}\text{Ar}$ data on feldspar from the Heilsberg bentonite.

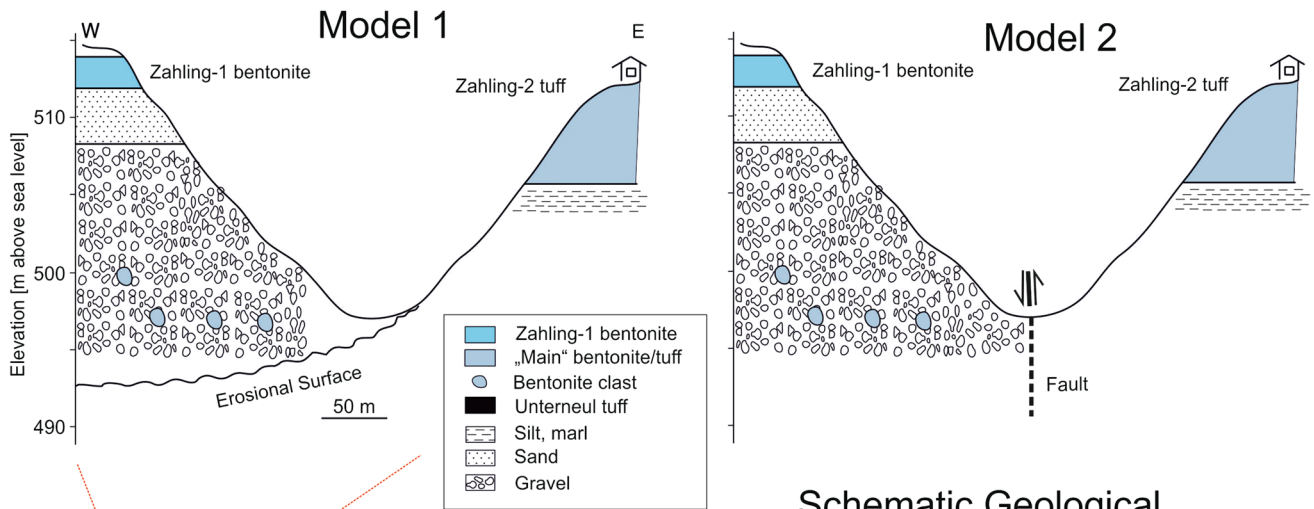
Interpretation of the U–Pb zircon ages: CA-ID-TIMS U–Pb zircon dating is considered to provide the most precise and accurate age information (e.g., Schaltegger et al. 2015). This appreciation is based on the well-known system behavior, the refractory nature of the host mineral and the high degree of analytical robustness and reliability. The age information from volcanic zircon needs, however, to be discussed in the light of possible protracted pre-eruptive residence in the magmatic reservoir (which can exceed

100 ka in felsic compositions; Reid et al. 1997), presence of xenocrystic material, and post-crystallization lead loss.

Zircon may crystallize in a magma reservoir over a period of several hundred thousand years, its saturation being controlled by temperature and the chemical composition of the melt (e.g., Barboni and Schoene 2014; Schoene et al. 2012; Wotzlaw et al. 2013). This implies that individual zircon crystals comprise growth zones of different age. Thus, in euhedral and not resorbed zircons, the rim most probably reflects the time of eruption. Bulk analysis of such a zircon by thermal ionization mass spectrometry (TIMS) will therefore result in integrated age information that is, however, biased toward the rim age by volume. Clustered youngest zircon dates from a volcanic system have been repeatedly shown to be a very reliable measure for the eruption age in most cases (e.g., Wotzlaw et al. 2014a).

Implications for the Ries meteorite impact: The Middle Miocene Ries crater at Nördlingen, southwest Germany, is one of the best-preserved and well-documented impact structures on Earth. Over the last 50 years, some 70 individual age determinations have been carried out on the basis of K–Ar, $^{40}\text{Ar}/^{39}\text{Ar}$, and fission-track-dating techniques. Investigated samples exclusively involved impact-generated glasses, i.e., solidified suevite melt and tektite (moldavite) melts. Recently published ages obtained by the $^{40}\text{Ar}/^{39}\text{Ar}$ technique range from <14.4 Ma (e.g., Buchner et al. 2010) to 14.88 ± 0.11 Ma (Aziz et al. 2008). Some of the data appear to be compromised by possible geochemical and/or analytical complications. Inaccurate data may arise from inherited Ar, K–Ar fractionation during alteration, recoil loss of ^{39}Ar during

Schematic Geological Section Zahling



Schematic Geological Section Unterneul

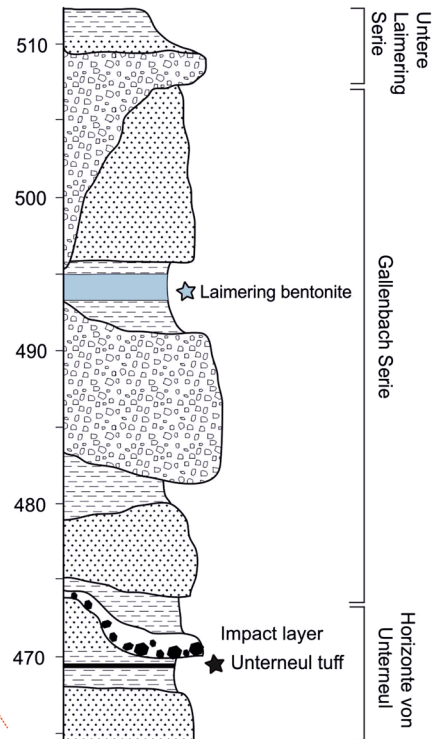


Fig. 5 Geological sketch of the Zahling-Unterneul-Laimering area and composite stratigraphic profile after Fiest (1989). The lithostratigraphic section indicates the position of the Unterneul and Laimering bentonites and the Brockhorizont impact layer intercalated with marls, sands and gravels. The different stratigraphic positions of the

Zahling-1 and Zahling-2 deposits, which share a common elevation above sea level but contrast significantly in age (age difference: 1.4 Ma) may be explained either by an erosional unconformity after Aziz et al. (2010; model 1) or tectonic displacement (model 2)

neutron irradiation and analytical issues such as imprecise estimates of ^{40}K decay constant, branching ratio, age of monitors (e.g., Kuiper et al. 2008; Renne et al. 2010, 2011). Our approach circumvents these problems

by applying Pb–U dating to zircons from altered tuff beds overlying (Laimering) and underlying (Unterneul) the impact-generated Brockhorizont. Our data suggest that the Ries impact occurred between 14.93 and 15.00 Ma,

and this date allocates the event to the astronomically tuned chron C5Bn1r (15.032–14.870 Ma; Hilgen et al. 2012). The suggested age is in accordance with paleomagnetic evidence, placing the Ries impact into a period of a reversed magnetic field (Pohl 1965, 1977). The U–Pb age further affirms the (recalculated) $^{40}\text{Ar}/^{39}\text{Ar}$ date of 14.98 ± 0.11 Ma obtained by Aziz et al. (2008) on Ries impact glasses, but it conflicts with recent estimates by Buchner et al. (2013). These authors recalculated published $^{40}\text{Ar}/^{39}\text{Ar}$ data using cross-calibrated monitor ages and the Renne et al. (2011) constants to suggest a slightly younger though statistically indistinguishable impact age of 14.74 ± 0.20 Ma. This date translates to 14.77 ± 0.20 Ma using the Min et al. (2000) and Kuiper et al. (2008) constants and FCs monitor age, respectively. The age difference of 100–200 ka is significant for paleontological research, paleoclimatic and paleoenvironmental reconstructions, as well as the calibration of bio- and magnetostratigraphic data. For example, the age proposed by Buchner et al. (2013) would allocate the Ries event to the next younger reversed chron (C5ADr), in contrast to the present and Aziz et al. (2008) studies (C5Bn1r). This conflict thus highlights the need for continuing research on the age of the Ries impact to establish the Brockhorizont as a firm stratigraphic anchor.

Implications for the Zahling deposits: Aziz et al. (2010) pointed out that two different bentonite tuff deposits exist at Zahling. Field observations assigned a younger stratigraphic age to the Zahling-1 bentonite (Fig. 5). This study underpins these conclusions. Although robust ages can be inferred neither for Zahling-1 nor -2 from the zircon analyses, the ^{238}U – ^{206}Pb dates for the youngest respective grains indicate a younger age for Zahling-1 by as much as 1.4 Ma.

The originally published $^{40}\text{Ar}/^{39}\text{Ar}$ age of 16.10 ± 0.22 Ma for Zahling-2 (Aziz et al. 2010) is in strong contrast to the ^{238}U – ^{206}Pb zircon date of 14.78 ± 0.14 Ma suggested here, the age difference most likely indicating a disturbance of the K–Ar system. The new date for Zahling-2 is no longer in line with a pre-Ries age proposed by Aziz et al. (2010), but consistent with the location of the Zahling-2 tuff about 20 m above the Brockhorizont (Schmid 1995). In fact, it is younger than the 14.925 ± 0.012 Ma ^{238}U – ^{206}Pb zircon age of the Laimering bentonite, 4 km to the SE, which is stratigraphically directly overlying the Brockhorizont (Fig. 5; Fiest 1989).

The apparent 1.4 Ma age difference between the Zahling-1 and Zahling-2 deposits is significant and fuels the discussion regarding the existence of a significant basin-wide hiatus in the Molasse basin. This sedimentary gap has been proposed on the results of geologic mapping at the northern rim of the Molasse basin (Birzer 1969), paleomagnetic data from Eastern Bavaria (Aziz et al. 2008), and biostratigraphic evidence (Böhme et al. 2002; Aziz et al.

2010) and was further supported by the originally suggested 16.1 Ma age for Zahling-2 (Aziz et al. 2010, their Fig. 15). The significantly younger age for the Zahling-2 tuff thus diminishes the need of a pre-Ries hiatus in Western Bavaria. Instead, such an age would rather point to a post-Ries hiatus between 14.78 (Zahling-2) and 13.34 Ma (Zahling-1), implying that at this location the complete Gallenbach Serie (sensu Fiest 1989) has been eroded or never been deposited (Fig. 5). A possible alternative interpretation would involve, instead of an erosional channel, a north–south trending fault between Zahling-1 and Zahling-2 (Fig. 5).

Aziz et al. (2010) interpreted the Zahling-1 bentonite as resting on gravel and sand strata belonging to the Gallenbach Serie. The suggested though not robust zircon age of around 13.3 Ma would, however, place the Zahling-1 gravels either into the younger Untere Laimering Serie or into the even younger Obere Laimering Serie (Fig. 5), the last sedimentary cycle of the region (Fiest 1989). The latter interpretation is supported by biostratigraphic data, which indicate no significant time gap between the Gallenbach and Untere Laimering Serie (Heissig 2006), but instead a long hiatus between the Untere and Obere Laimering Serie (Fiest 1989; Heissig 1989). The only observed fauna of the Untere Laimering Serie is found at their base in Laimering 5 (Heissig 2006). This fauna contains, beside others, the rodent *Cricetodon aureus*. This species has also been found at the top of the Gallenbach Serie at Laimering 4b (Rummel 2000; Heissig 2006) where it directly overlies the Laimering bentonite dated at 14.925 ± 0.01 Ma. The Obere Laimering Serie contains the fauna of Laimering 1a, which is biostratigraphically significantly younger (Heissig 1989; Bolliger 1994). The presence of *Megacricetodon similis* is shared with several Swiss localities dated to between 14 and 13 Ma (Kälin and Kempf 2009). In conclusion, zircon ages of the Zahling tuffs support the existence of a long hiatus between the Untere and Obere Laimering Serie.

Correlation of OSM tuffs with Swiss, Italian, Austrian, Hungarian and Romanian occurrences: A wealth of age data is now available for Middle Miocene tephra layers from Central Europe allowing for a first, preliminary correlation scheme across the continent. Our new U–Pb zircon data indicate eruption ages of 13.34 ± 0.39 Ma (Zahling-1), 14.417 ± 0.009 Ma (Bischofszell), 14.772 ± 0.032 Ma (Hachelstuhl), 14.78 ± 0.14 Ma (Zahling-2), 14.925 ± 0.012 Ma (Laimering), 15.003 ± 0.024 Ma (Unterneu), 15.120 ± 0.083 Ma (Krumbad) and 15.32 ± 0.02 Ma (Ponholz). The zircon ages are complemented by revised $^{40}\text{Ar}/^{39}\text{Ar}$ data for Heilsberg feldspar (14.63 ± 0.14 Ma). Gubler et al. (1992) and Gubler (2009) presented U–Pb zircon ages for four bentonite horizons in the Zurich area, Switzerland, namely 14.20 ± 0.08 Ma (Leimbach), 14.29 ± 0.10 Ma (Aeugstertal), 14.91 ± 0.09

and 14.84 ± 0.07 Ma (Küsnacht), and 15.27 ± 0.12 and 15.31 ± 0.05 Ma (Urdorf). Note, however, that the ages reported in Gubler (2009) are partially based on provisory data from an unpublished NAGRA report for which no analytical details exist (Nagra 2008). Handler et al. (2006) provide $^{40}\text{Ar}/^{39}\text{Ar}$ feldspar and biotite ages for Miocene tuffs from the Styrian Basin at the western end of the Pannonian Basin that we recalculated according to updated monitor and decay parameters as explained above. The new $^{40}\text{Ar}/^{39}\text{Ar}$ ages are 14.30 ± 0.07 , 14.48 ± 0.12 , 15.18 ± 0.09 , and 15.32 ± 0.17 Ma. From the Carpathian-Pannonian area, single zircon ages obtained by LA-ICP-MS are reported by Lukács et al. (2015) for various tephra layers of the Upper Rhyolite Tuff unit drilled at the Bükkalya Volcanic Field, Hungary. The authors distinguish four eruptive phases from 15.9 to 14.1 Ma, each of which possibly including multiple eruptive events. Additional ages of acidic volcanic products in the Carpathian-Pannonian region, ranging between 11 and 15 Ma, are based on the K–Ar method (e.g., Márton and Pécskay 1998; Szakács et al. 1998; Fülöp and Kovacs 2003; Pécskay et al. 2006). Further East in the Transylvanian Basin, the Romanian Dej Tuff unit has been recently dated by $^{40}\text{Ar}/^{39}\text{Ar}$ at 14.37 ± 0.06 Ma (de Leeuw et al. 2013) and 14.8–15.1 Ma (Szakács et al. 2012), respectively. Furthermore, complementary astrochronological (Hilgen et al. 2003; Hüsing et al. 2009, 2010; Turco et al. 2017) and high-precision U–Pb zircon data (Wotzlaw et al. 2014b) have been obtained from tuff bands in marine sediment successions at Monte dei Corvi and La Vedova near Ancona, Italy, with 8 out of 17 tuff horizons erupted in the time range of interest (13–15.5 Ma). The La Vedova data probably represent the closest approach to “absolute” ages for the time window discussed and therefore serve as a reference frame for a tentative Middle Miocene tephrochronology in southern Central Europe. All ages are displayed in Fig. 6 and grouped with respect to their regional occurrence. Figure 7 shows a very first and only preliminary approach to correlate the various Middle Miocene tephra beds across Central Europe. A precondition of this concept is a common source of correlated volcanic units. For the time window discussed, the Carpathian-Pannonian volcanic field appears to be the only source region for explosive calc-alkaline felsic magmatism (Unger et al. 1990) with pyroclastic rocks being produced between 21 and 11 Ma (Márton and Pécskay 1998; Szakács et al. 1998; Pécskay et al. 2006; Lukács et al. 2015). The genetic link between several bentonites and tuffs from the Pannonian and Molasse basin has been suggested using geochemical data (Unger and Niemeyer 1985b, 1990).

In a first approach, we discuss our data in a preliminary European correlation scheme (Figs. 6, 7) which is mainly based on tephra ages but also considers information from local geology, geochemistry and paleomagnetic

systematics. Note that due to the large uncertainty of various data and/or possible prolonged residence times of zircons in their magma reservoirs the suggested correlations are partly speculative and require confirmation by geochemical, mineralogical, isotopic and/or paleomagnetic data. The tuffs will be discussed in stratigraphic order. The correlation scheme contains the following elements:

- The oldest altered tephra dated in this study, the Weisse Lasse tonstein from Ponholz (15.32 ± 0.02 Ma), is identical in age with the Urdorf bentonite in Switzerland (15.31 ± 0.05 Ma) and a tuff layer Hörmsdorf-2 from the Middle Eibiswald Formation in the Styrian Basin at the western border of the Pannonian Basin (15.32 ± 0.17 Ma).
- Due to the large analytical uncertainty, the true age and stratigraphic position of the Krumbad bentonite (15.12 ± 0.22 Ma) is ambiguous. It may be allocated to either the Hörmsdorf 2-Ponholz-Urdorf event, to one of the nominally younger bentonites such as Unterneul, Laimering (see below) or Hörmsdorf-1 (15.18 ± 0.09 Ma), or neither of them. Note that despite overlapping ages the distinct chemical compositions of residual fresh glass fragments in Krumbad and Zahling-2 tuffs seem to argue against a common origin. Both the major element composition and trace element systematics of Krumbad glasses are identical or very similar to that of other Lower Bavarian bentonites (e.g., Hachelstuhl, Birnfeld, Martinszell, Niederreith, Malgersdorf) but seemingly distinct from that of Zahling-2, Bischofszell and Heilsberg representing a second compositional group (Gilg 2005; Aziz et al. 2010). Alternatively, the systematically lower K₂O contents of Bischofszell glasses may indicate a third compositional group. Overall, these observations may be interpreted as the successive reactivation of distinct volcanic centers through time, but the possibility of a mineralogically and chemically zoned magma chamber may also be considered (Hildreth and Wilson 2007). The problem can only be unambiguously solved by a refined dating of the Krumbad bentonite. Because of its large uncertainty in age, we hesitate to suggest any correlation for the Krumbad bentonite.
- Unterneul (15.003 ± 0.024 Ma) and Laimering (14.925 ± 0.012 Ma) bentonites are underlying and overlying the Brockhorizont, respectively (Fig. 5), assigning the Ries impact to the astronomically tuned chron C5Bn1r (14.87 – 15.032 Ma; Hilgen et al. 2012), in accordance to paleomagnetic evidence (Pohl 1977; Pohl et al. 2010). The paleomagnetic data also suggest that the switch from reverse chron C5Bn1r to normal chron C5Bn1n occurred immediately after the Ries impact and may have even been triggered by it. This would

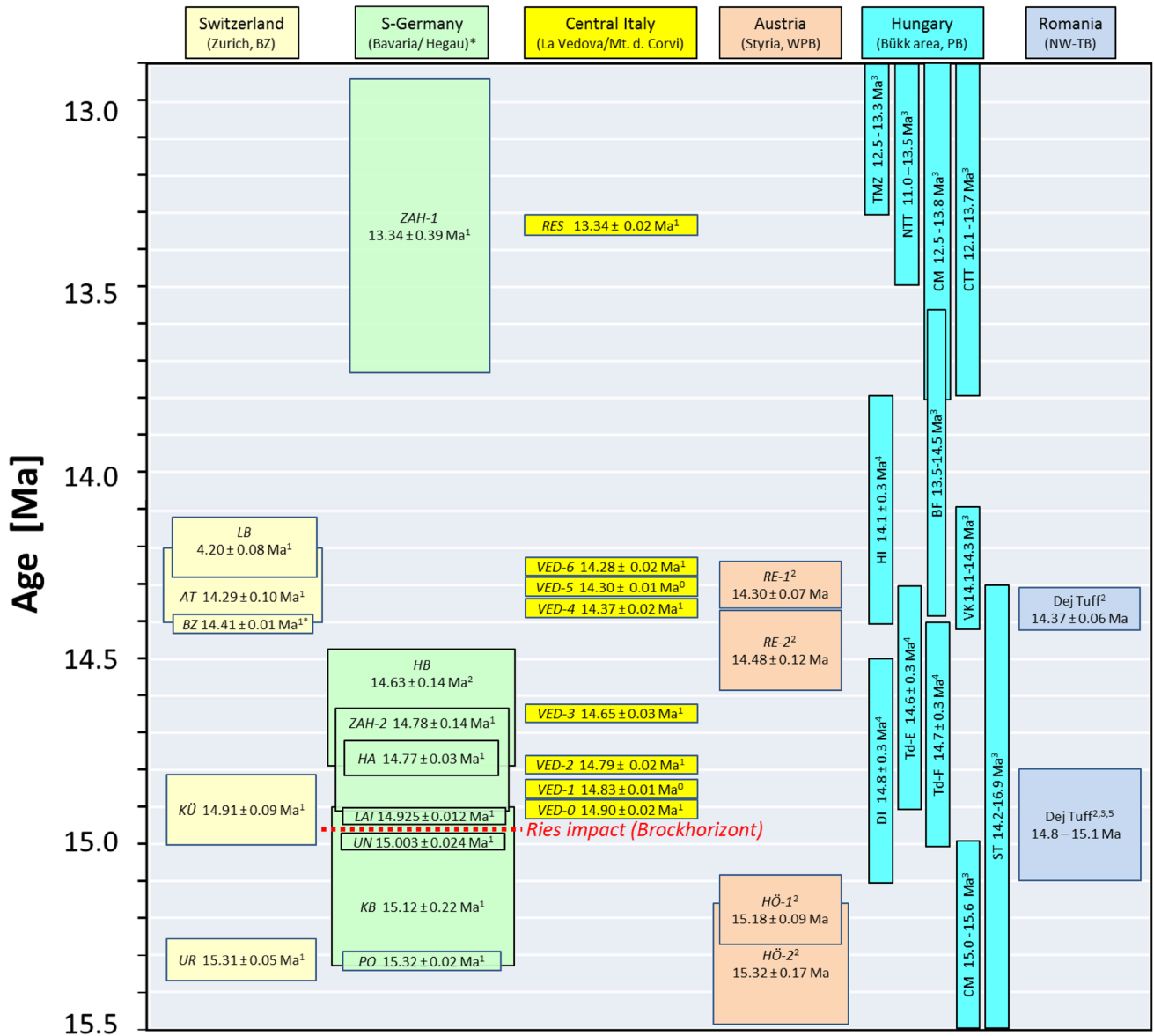


Fig. 6 Isotopic (single zircon U–Pb, $^{40}\text{Ar}/^{39}\text{Ar}$, K–Ar) and astronomical ages of rhyolitic tephra beds in Central Europe and Italy arranged from West to East. Errors represent 2-sigma errors. $^{40}\text{Ar}/^{39}\text{Ar}$ ages are corrected for revised decay constants and FCs monitor age (see text). CPB Eastern Pannonian Basin, WPB Western Pannonian Basin, NW-TB Northwestern Transylvanian Basin, ZAH Zahling, HB Heilsberg, HA Hachelstuhl, LAI Laimering, UN Unterneul, KB Krumbad, PO Ponholz, LB Leimbach, AT Aegustertal, BZ Bischofszell, KÜ Küsnacht, UR Urdorf, RES and VED-0 to VED-6: tephra layers at Monte dei Corvi and La Vedova, respectively; RE Retznei, HÖ Hörnsdorf, TMZ Tokay-Milic-Zemplin, NTT Northern Trans-Tisza

region, CM Cserhát-Matrâ, CTT Central Trans-Tisza region, BF Bükk Foreland, ST Southern Transdanubia, VK Vtáčnik-Kremnické vrehy. 0: astronomical ages; 1 single zircon U/Pb ages, 2 $^{40}\text{Ar}/^{39}\text{Ar}$ mineral ages, 3 K–Ar mineral ages, 4 LA-ICP-MS ages, 5 fission-track ages (zircons). Data source for Central Italy: Hüsing et al. (2010) in Wotzlav et al. (2014a); Switzerland: Gubler et al. (1992), Gubler (2009), this study (Bischofszell); South Germany: this study, Aziz et al. (2010); Styria/WPB: Handler et al. (2006); Hungry/CPB: Lukács et al. (2015), Pécskay et al. (2006); Romania/NW-TB: de Leeuw et al. (2013), Szakács et al. (2012)

suggest placing the impact event close to 14.9 Ma, the underlying Unterneul bentonite into the reversed chron C5Bn1r and the overlying Laimering bentonite into the normal chron C5Bn1n.nn

At La Vedova, Italy, two tuff beds overlap with astronomically defined time window of the Ries event:

VED-0 (with an astronomical age of 14.884 Ma and a weighted mean $^{206}\text{U}/^{238}\text{Pb}$ age of 14.9025 ± 0.021 Ma) and VED-1 (with an astronomical age of 14.834 Ma; a weighted mean $^{206}\text{U}/^{238}\text{Pb}$ age is not reported; Wotzlav et al. 2014a). Provided that the Unterneul and Laimering eruption events are also visible at

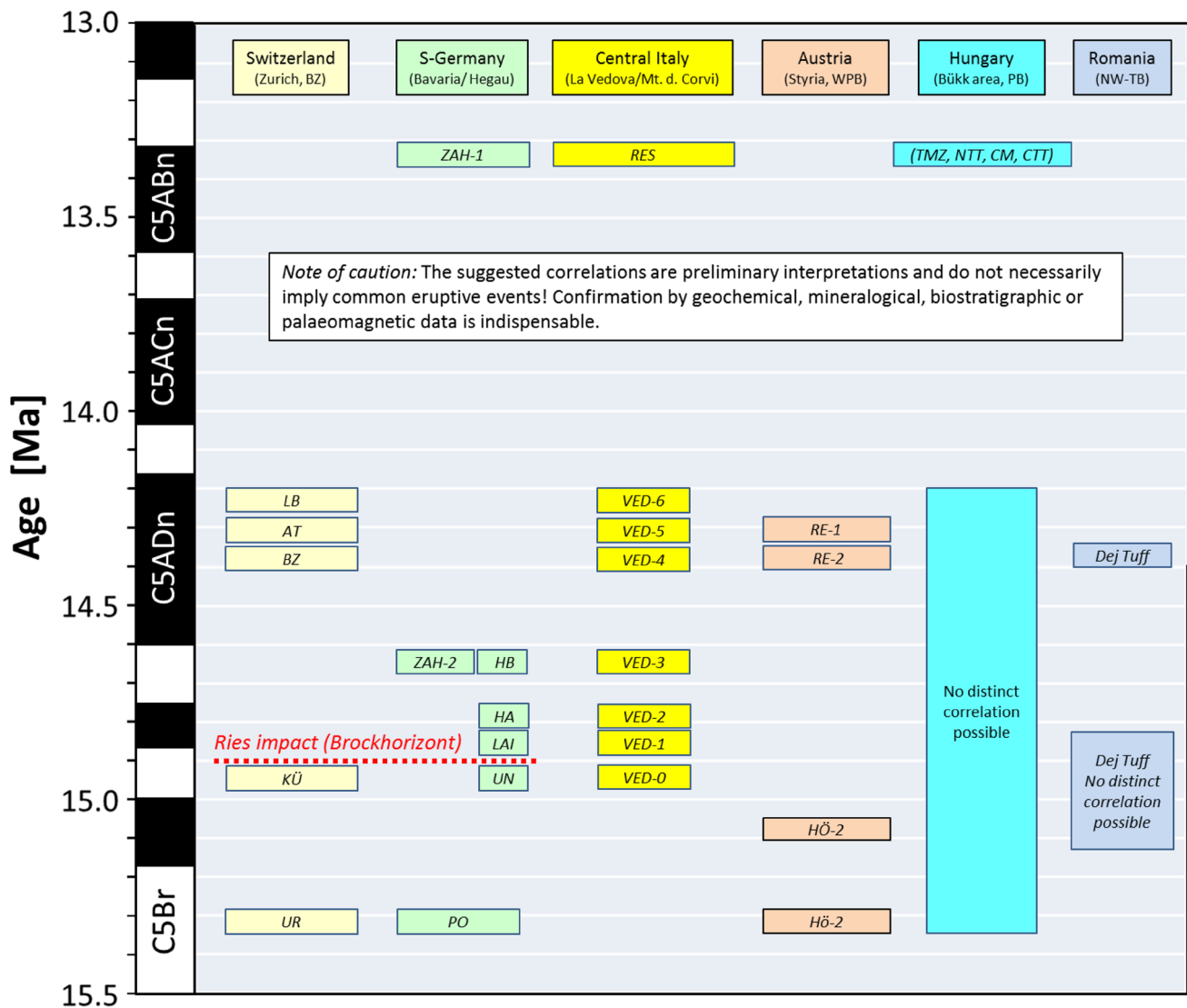


Fig. 7 Preliminary correlation scheme for Middle Miocene Central European tuff horizons based on Fig. 6. The assumed correlations should be considered as first approximations only. The model rests on the assumption that during the Middle Miocene the Carpathian–Pannonian volcanic field was the only source region for explosive acidic volcanism and its pyroclastic products in Central Europe (see text). The model suggests that Plinian ash erupting in the Pannonian

Basin were transported for more than 1000 km to the west and represent efficient marker horizons. Because of its large uncertainty in age KB (Krumbad) has not been taken in account. The long-lasting and continuous volcanic activity in the assumed Pannonian source region inhibits conclusive correlation to tephra layers in Western Europe. Abbreviations, see Fig. 6

La Vedova, we suggest that the older of the two La Vedova tuffs, VED-0 correlates with Unterneul, and the ca. 50 ka younger VED-1 tuff with Laimering. This interpretation is in accord with the roughly similar age difference between the respective younger and older tuffs at both localities (50 ka at La Vedova vs. 80 ± 40 ka at Unterneul/Laimering). It is also in perfect agreement with paleomagnetic systematics. The magnetic polarities of VED-0 and VED-1 and their fit to the magnetostratigraphic column mirror the situation at Unterneul and Laimering as outlined above, with

VED-0 and VED-1 being allocated to C5Bn.1r and C5Bn.1n, respectively (Hüsing et al. 2010; Wotzlaw et al. 2014b). The suggested correlation requires, however, protracted residence times of zircon in the respective magma chambers for Unterneul, Laimering and VED-1. Prolonged residence of zircon is common in felsic magmas and may in some cases exceed 100 ka (Reid et al. 1997). This is in fact indicated for VED-1 where even the youngest $^{206}\text{Pb}/^{238}\text{U}$ date is not only older than the stratigraphically underlying VED-0 tuff, but also exceeding the astronomical age by 100 ka

(Wotzlaw et al. 2014a). Another hint for the suggested correlations is given by the similar Th/U ratios in the respective zircon populations, with Laimering and VED-1 having consistently elevated values as compared to Unterneul and VED-0 (Wotzlaw et al. 2014b).

- One tuff horizon from the Zurich area, the Künsnacht bentonite, falls into the Ries age range. Gubler et al. (1992) and Gubler (2009) report U–Pb zircon ages of 14.91 ± 0.09 and 14.84 ± 0.05 Ma, respectively. As the Künsnacht bentonite is interpreted to be situated some 20–30 m below the Ries ejecta (Kälin and Kempf 2009), we adopt the older age and allocate the Künsnacht to the Unterneul bentonite.
- The main bentonite horizon in the Landshut area at Hachelstuhl (14.772 ± 0.032 Ma) is matched either by VED-2 with U–Pb and astronomical ages of 14.787 ± 0.021 and 14.720 Ma, respectively, or, less likely, by the slightly older VED-1 tuff, for which only an astronomical age of 14.834 Ma exists.
- Due to the large uncertainties, the tuffs of Zahling-2 (14.78 ± 0.14 Ma) and Heilsberg (14.63 ± 0.14 Ma, $^{40}\text{Ar}/^{39}\text{Ar}$ feldspar age) could be related to either tuff VED-3 (14.654 and 14.649 ± 0.031 Ma, respectively) or the earlier Hachelstuhl and VED-2 event. We prefer here the first interpretation, as the glasses from Zahling-2 and Heilsberg show identical chemical compositions, which are distinct from that of the Hachelstuhl glasses (Gilg 2005; Aziz et al. 2010). Additionally, both samples from Zahling-2 and Heilsberg contain a characteristic magmatic plagioclase that is not found in the Hachelstuhl tuff.
- The Bischofszell bentonite (14.417 ± 0.009 Ma) may possibly be matched by VED-4 (14.356 and 14.368 ± 0.21 Ma, respectively), Retznei-2 (Styria) and Dej Tuff in Romania. The $^{40}\text{Ar}/^{39}\text{Ar}$ analyses of sanidine by de Leeuw et al. (2013) date the Dej Tuff at 14.37 ± 0.06 Ma. Note that this age contrasts with the rather unspecific 14.8–15.1 Ma range suggested by Szakács et al. (2012). The latter data were obtained on the basis of combined fission-track analyses of zircons and K–Ar dating of biotite, both methods with large analytical scatter. Because of their large spread, we do not use these data for correlation purposes. The eruption center of the Dej Tuff is inferred to be located outside the Transylvanian Basin, possibly in the Western Gutâi Mountain area in Northern Romania (Szakács et al. 2000). If the Bischofszell bentonite is indeed related to the Dej Tuff, a stratigraphic East–West traceability of more than 1100 km may be postulated for this eruption, implying ash transport by stratospheric winds.
- Both the VED-5 (astronomical age 14.300 Ma; no $^{206}\text{Pb}/^{238}\text{U}$ age reported) and VED-6 tuffs (14.257 and 14.275 ± 0.021 Ma, respectively) may be correlated with the Aegustertal bentonite in Switzerland (14.29 ± 0.10 Ma; Gubler 2009). Further to the east, this event may be matched by the Retznei-1 tuff in the Styrian Basin dated by $^{40}\text{Ar}/^{39}\text{Ar}$ (biotite, sanidine) at 14.30 ± 0.07 Ma (Handler et al. 2006).
- The 13.34 ± 0.39 Ma age of Zahling-1 is only constrained by the youngest zircon. It is identical to the age of the RES tuff in Italy (13.34 ± 0.02 Ma; Wotzlaw et al. 2014a). No other correlation to any western European tuff horizon is suggested by the data. Note, however, that the contrasting zircon age distribution in Zahling-1 (age spread 1.2 Ma) and RES tuffs (age spread 60 ka) may suggest that these two tuffs are possibly different and thus not correlated.
- Both the published K–Ar (Pécskay et al. 2006) and U–Pb (Lukács et al. 2015) age data on rhyolitic tephra/tuffs from the Carpathian–Pannonian area in Hungary support the notion that long-lived silicic magma reservoirs existed in the Pannonian Basin during the Middle Miocene and that eruptive phases probably included multiple eruptive events (e.g., Lukács et al. 2015; Seghedi et al. 2004).

The correlation scheme shown in Fig. 7 tolerates the 0–150 ka offset between astronomical and U–Pb ages in the La Vedova and Monte dei Corvi data set (Wotzlaw et al. 2014a), which is probably mainly caused by prolonged residence times of zircons in their magma reservoirs. While some of the correlations in the diagram appear firm (though not proving genetic relationships between the tuffs!), others should be considered speculative at best. Also keep in mind that tuffs deposited in the Molasse basin not necessarily have to be found in the Adriatic Sea or elsewhere, and vice versa. This first European Middle Miocene tephrochronology scheme undoubtedly requires improvements by additional high-quality ages and complementary geochemical, mineralogical, isotopic and paleomagnetic data.

Conclusions

New U–Pb zircon ages, together with revised $^{40}\text{Ar}/^{39}\text{Ar}$ ages published in Aziz et al. (2008, 2010) of bentonite and tuff layers, provide new stratigraphic time markers within the clastic sedimentary strata of Middle Miocene Upper Freshwater Molasse in Switzerland and southern Germany including the lignite-bearing units of the Paleo-Naab system. Within 2-sigma error, the new U–Pb ages overlap with the revised $^{40}\text{Ar}/^{39}\text{Ar}$ data at Hachelstuhl and Krumbad, but differ by more than 1.4 Ma at Zahling. The discrepancy is attributed to open system behavior of the fine-walled glass

fragments during alteration and/or neutron irradiation (recoil loss of ^{39}Ar). As this problem may possibly be omnipresent in pumice analysis, we consider the $^{40}\text{Ar}/^{39}\text{Ar}$ data obtained on glass shards as less reliable than the respective U–Pb zircon data. The $^{40}\text{Ar}/^{39}\text{Ar}$ age of feldspar from the Heilsberg bentonite, however, is considered as firm.

The new data, in combination with high-quality ages of tephra horizons from Central Italy (Wotzlaw et al. 2014a), Swiss Molasse (Gubler et al. 1992; Gubler 2009), Styrian Basin (Handler et al. 2006), Carpathian-Pannonian region (Pécskay et al. 2006; Lukács et al. 2015) and Transylvanian Basin (Romania; Szakács et al. 2012; de Leeuw et al. 2013); allows for a first approach in correlating tuff horizons across Central Europe and Italy ranging in the age between roughly 13 and 15.5 Ma. Due to their wide-spread distribution in Central Europe, the Middle Miocene tephra from Carpathian–Pannonian volcanoes are considered to be ideal tracers for constructing a supra-regional correlation. The suggested Middle Miocene tephrochronology scheme is a very first step toward this goal, but requires refinement and/or corrections by additional high-quality ages and complementary isotope, geochemical, mineralogical and paleomagnetic data.

U–Pb zircon ages of Laimering and Unterneul bentonite tuffs over- and underlying the clastic Brockhorizont (ejecta of the Ries meteorite impact) allocate the Ries event to chron C5Bn1r (15.032–14.870 Ma). Such an age is in accordance with geomagnetic evidence and approves the (recalculated) 14.98 ± 0.11 Ma $^{40}\text{Ar}/^{39}\text{Ar}$ date of Ries impact glasses (Aziz et al. 2008). It exceeds, however, recent estimates by Buchner et al. (2013), who exclusively considered $^{40}\text{Ar}/^{39}\text{Ar}$ ages of impact melts/glasses, by some 100–200 ka. This age difference on this important marker horizon is significant with respect to required temporal resolution in modern geoscientific research. It may be due to the different material investigated or to the different methods applied or both. The conflict highlights the need for future research on the age of the Ries impact to establish the Brockhorizont as a stratigraphic anchor.

Acknowledgements All samples, except that from Ponholz, were provided by A. Ulbig. The analytical work of M. Ovtcharova (University of Geneva) in the laboratory at University of Geneva is highly appreciated. We are grateful for the very helpful comments and constructive criticism by Ioan Seghedi, Wilfried Winkler and Jörn-Fredrik Wotzlaw and wish to acknowledge editorial handling by Christian Dullo. Initial financial support was provided by the German Science Foundation project BO1550/7.

References

- Aziz HA, Böhme M, Rocholl A, Zwing A, Prieto J, Wijbrans JR, Heissig K, Bachtadse V (2008) Integrated stratigraphy and $^{40}\text{Ar}/^{39}\text{Ar}$ chronology of the early to Middle Miocene upper freshwater Molasse in eastern Bavaria (Germany, Bavaria). *Int J Earth Sci (Geol Rundsch)* 97:115–134
- Aziz HA, Böhme M, Rocholl A, Prieto J, Wijbrans JR, Bachtadse V, Ulbig A (2010) Integrated stratigraphy and $^{40}\text{Ar}/^{39}\text{Ar}$ chronology of the early to middle Miocene Upper Freshwater Molasse in western Bavaria (Germany). *Int J Earth Sci (Geol Rundsch)* 99:1859–1886
- Barboni M, Schoene B (2014) Short eruption window revealed by absolute crystal growth rates in a granitic magma. *Nat Geosci* 7:524–528
- Bauer KK, Vennemann TW, Gilg HA (2016) Stable isotope composition of bentonites from the Swiss and Bavarian Freshwater Molasse as a proxy for paleoprecipitation. *Palaeogeogr Palaeoclimatol Palaeoecol* 455:53–64
- Birzer F (1969) Molasse und Ries-Schutt im westlichen Teil der südlichen Frankenalb. *Geologische Blätter Nordost-Bayern* 19:1–28
- Black LP, Kamo SL, Allen CM, Davis DW, Aleinikoff JN, Valley JW et al (2004) Improved $^{206}\text{Pb}/^{238}\text{U}$ microprobe geochronology by the monitoring of a trace-element-related matrix effect; SHRIMP, ID-TIMS, ELA-ICP-MS and oxygen isotope documentation for a series of zircon standards. *Chem Geol* 205:115–140
- Böhme M, Gregor H-J, Heissig K (2002) The Ries- and Steinheim meteorite impacts and their effect on environmental conditions in time and space. In: Buffetaut E, Koerbel C (eds) *Geological and biological effects of impact events*. Springer, Berlin, pp 215–235
- Bohor BF, Triplehorn DM (1993) Tonsteins: altered volcanic ash layers in coal-bearing sequences. *Geol Soc Am Spec Pap* 285:1–44
- Bolliger T (1992) Kleinsäugerstratigraphie in der lithologischen Abfolge der miozänen Hörnlischüttung (Ostschweiz) von MN3 bis MN7. *Ecol Geol Helvet* 85:961–1000
- Bolliger T (1994) Die Obere Süßwassermolasse in Bayern und der Ostschweiz: bio- und lithographische Korrelationen. *Mitt Bayer St-Samml Paläont Hist Geol* 34:109–144
- Bowring JF, Mclean NM, Bowring SA (2011) Engineering cyber infrastructure for U–Pb geochronology: Tripoli and U–Pb_Redux. *Geochem Geophys Geosyst* 12:Q0AA19
- Brasier MD, Matthewman R, McMahon S, Wacey D (2011) Pumice as a remarkable substrate for the origin of life. *Astrobiology* 11(7):725–735
- Buchner E, Schwarz WH, Schmieder M, Trieloff M (2010) Establishing a 14.6 ± 0.2 Ma age for the Nordlinger Ries impact (Germany)—a prime example for concordant isotopic ages from various dating materials. *Meteorit Planet Sci* 45:662–674
- Buchner E, Schmieder M, Schwarz WH, Trieloff M (2013) Das Alter des Meteoritenkraters Nördlinger Ries - eine Übersicht und kurze Diskussion der neueren Datierungen des Riesimpakts. *Z Dt Ges Geowiss (German J Geosci)* 164(3):433–445
- Bürgisser HM (1980) Zur Mittel-Miozänen Sedimentation im nordalpinen Molassebecken: das ‘Appenzellergranit’- Leitniveau des Hörnli-Schuttfächers (OSM, Nordostschweiz). *Mitt Geol Inst ETH Univ Zürich NF* 232:1–196
- Cerling TE, Brown FH, Bowman JR (1985) Low-temperature alteration of volcanic glass: hydration, Na, K, ^{18}O and Ar mobility. *Chem Geol Isot Geosci Sect* 52:281–293
- Channell JET, Hodell DA, Singer BS, Xuan C (2010) Reconciling astrochronological and $^{40}\text{Ar}/^{39}\text{Ar}$ ages for the Matuyama–Brunhes boundary and late Matuyama Chron. *Geochem Geophys Geosyst* 11:1–21
- Condon D, Mclean N, Schoene B, Bowring S, Parrish R, Noble SR (2008) Synthetic U–Pb ‘standard’ solutions for ID-TIMS geochronology. *Geochim Cosmochim Acta* 72:A175–A1751
- Condon DJ, Schoene B, McLean NM, Bowring S, Parrish RR (2015) Metrology and traceability of U–Pb isotope dilution

- geochronology (EARTHTIME Tracer Calibration Part I). *Geochim Cosmochim Acta* 164:464–680
- Crowley JL, Schoene B, Bowring SA (2007) U-Pb dating of zircon in the Bishop Tuff at the millennial scale. *Geology* 35(12):1123
- de Leeuw A, Filipescu S, Matenco L, Krijgsman W, Kuiper K, Stoica M (2013) Paleomagnetic and chronostratigraphic constraints on the Middle to Late Miocene evolution of the Transylvanian Basin (Romania): implications for Central Paratethys stratigraphy and emplacement of the Tisza–Dacia plate. *Glob Planet Chang* 103:82–98
- Dehm R (1951) Zur Gliederung der jungtertiären Molasse in Süddeutschland nach Säugetieren. *N Jb Geol Pal Mh* 1951:140–152
- Doppler G (1989) Zur Stratigraphie der nördlichen Vorlandmolasse in Bayerisch-Schwaben. *Geol Bavarica* 94:83–133
- Doppler G, Heissig K, Reichenbacher B (2005) Die Gliederung des Tertiärs im süddeutschen Molassebecken. *Newslett Stratigr* 41:359–375
- Fiest W (1989) Lithostratigraphie und Schwermineralgehalt der Mittleren und Jüngeren Serie der Oberen Süßwassermolasse Bayerns im Übergangsbereich zwischen Ost- und Westmolasse. *Geol Bavarica* 94:259–279
- Fischer H (1988) Isotopengeochemische Untersuchungen und Datierungen an Mineralien und Fossilien aus Sedimentationsgesteinen. Diss, ETH Zürich, p 8733
- Fülöp A, Kovacs M (2003) Petrology of Badenian ignimbrites, Gutái Mts. (Eastern Carpathians) *Studia Univ Babeş-Bolyai. Geol* 48:17–28
- Gerstenberger H, Haase G (1997) A highly effective emitter substance for mass spectrometric Pb isotope ratio determinations. *Chem Geol* 136:309–312
- Gilg HA (2005) Eine geochemische Studie an Bentoniten und vulkanischen Gläsern des nordalpinen Molassebeckens (Deutschland, Schweiz). *Ber DTTG* 11:17–19
- Gilg HA, Ulbig A (2017) Bentonite, Kohlensteine und feuerfeste Tone in der Bayerischen Molasse und dem Urnaab-System (Exkursion F am 20. April 2017). *Jber Mitt Oberrhein Geol Ver N.F.* 99:191–214
- Gubler T (2009): Blatt 1111 Albis (mit Beitrag von P. Nagy). *Geol. Atlas Schweiz* 1: 25 000, Erläut: 134. Bundesamt für Landestopographie swisstopo
- Gubler T, Meier M, Oberli F (1992) Bentonites as time markers for sedimentation of the Upper Freshwater Molasse: geological observations corroborated by high-resolution single-Zircon U–Pb ages. 172. *Jv Schweiz Akad Naturwiss* 12–13
- Handler R, Ebner F, Neubauer F, Bojar A-V, Hermann S (2006) $^{40}\text{Ar}/^{39}\text{Ar}$ dating of Miocene tuffs from the Styrian part of the Pannonian Basin: an attempt to refine the basin stratigraphy. *Geol Carpathica Bratislava* 57(6):483–494
- Harr K (1976) Mineralogisch-petrographische Untersuchungen an Bentoniten in der Süddeutschen Molasse. PhD thesis, University Tübingen, 135
- Heissig K (1989) Neue Ergebnisse zur Stratigraphie der Mittleren Serie der Oberen Süßwassermolasse Bayerns. *Geol Bavarica* 94:239–258
- Heissig K (1997) Mammal faunas intermediate between the reference faunas of MN4 and MN6 from the Upper Freshwater Molasse of Bavaria. In: Aguilar JP, Legendre S, Michaux J (eds), *Actes du Congrès Biochron’97–Mémoires et Travaux* 21. Montpellier: de l’Ecole Pratique des Hautes Etudes, Institute de Montpellier, 537–546
- Heissig K (2006) Biostratigraphy of the “main bentonite horizon” of the upper freshwater molasses in Bavaria. *Palaeontogr A* 277:93–102
- Hildreth W, Wilson JN (2007) Compositional zoning of the Bishop Tuff. *J Petrol* 48:951–999
- Hilgen FJ, Aziz HA, Krijgsman W, Raffi I, Turco E (2003) Integrated stratigraphy and astronomical tuning of the Serravallian and lower Tortonian at Monte dei Corvi (Middle-Upper Miocene, northern Italy). *Palaeogeogr Palaeoclimatol Palaeoecol* 199(3–4):229–264
- Hilgen FJ, Lourens LJ, Van Dam JA (2012) The Neogene period. In: Gradstein FM, Ogg JG, Schmitz MD, Ogg GM (eds) *The geological time scale 2012*. Elsevier, Amsterdam, pp 923–978
- Hofmann F (1956) Sedimentpetrographische und tonmineralogische Untersuchungen an Bentoniten der Schweiz und Südwestdeutschlands. *Eclog Geol Helvet* 49:113–133
- Hofmann F (1958) Vulkanische Tuffhorizonte in der Oberen Süßwassermolasse des Randen und Reiat, Kanton Schaffhausen. *Eclog Geol Helvet* 51:371–377
- Hofmann F (1973) Horizonte fremdartiger Auswürfling in der ostschweizerischen Oberen Süßwassermolasse und Versuch einer Deutung ihrer Entstehung als Impact phänomen. *Eclog Geol Helvet* 66:83–100
- Hofmann F, Büchi UP, Iberg R, Peters TJ (1975) Vorkommen, petrographische, tonmineralogische und technologische Eigenschaften von Bentoniten im schweizerischen Molassebecken. *Beitr Geol Karte der Schweiz, Geotechn Serie* 54:1–51
- Homewood P, Allen PA, Williams GD (1986) Dynamics of the Molasse Basin of Western Switzerland. In: Allen PA, Homewood P (eds), *Foreland basins vol. 8. Spec Publ Int Assoc Sedimentol*, Blackwell Pub, Oxford, pp 199–217
- Hüsing SK, Dekkers MJ, Franke C, Krijgsman W (2009) The Tortonian reference section at Monte dei Corvi (Italy): evidence for early remanence acquisition in greigite-bearing sediments. *Geophys J Int* 179(1):125–143
- Hüsing SK, Cascella A, Hilgen FJ, Krijgsman W, Kuiper KF, Turco E, Wilson D (2010) Astrochronology of the Mediterranean Langhian between 15.29 and 14.17 Ma. *Earth Planet Sci Lett* 290:254–269
- Jaffey AH, Flynn KF, Glendenin LE, Bentley WC, Essling AM (1971) Precision measurement of half-lives and specific activities of ^{235}U and ^{238}U . *Phys Rev* 4:1889–1906
- Jicha BR, Singer BS, Sobol P (2016) Re-evaluation of the ages of $^{40}\text{Ar}/^{39}\text{Ar}$ sanidine standards and supereruptions in the western US using a Noblesse multi-collector mass spectrometer. *Chem Geol* 431:54–66
- Jordan F, Matzel JP, Renne PR (2007) ^{39}Ar and ^{37}Ar recoil loss during neutron irradiation of sanidine and plagioclase. *Geochim Cosmochim Acta* 71:2791–2808
- Kälin D, Kempf O (2009) High-resolution stratigraphy from the continental record of the Middle Miocene Northern Alpine Foreland Basin of Switzerland. *N Jb Geol Paläont Abh* 254:177–235
- Karner DB, Juvigne E, Brancaccio L, Cinque A, Ermolli ER, Santangelo N, Bernasconi S, Lirer L (1999) A potential early middle Pleistocene tephrostratotype for the Mediterranean basin: the Vallo Di Diano, Campania, Italy. *Glob Planet Chang* 21:1–15
- Köster MH, Gilg HA (2015) Pedogenic, palustrine and groundwater dolomite formation in non-marine bentonites (Bavaria, Germany). *Clay Miner* 50:163–183
- Kromer H (1980) Tertiary clays in northeastern Bavaria (Oberpfalz). *Geol Jb D* 39:25–45
- Kuhlemann J, Kempf O (2002) Post-Eocene evolution of the North Alpine Foreland Basin and its response to Alpine tectonics. *Sediment Geol* 152:45–78
- Kuiper KF, Deino A, Hilgen FJ, Krijgsman W, Renne PR, Wijbrans JR (2008) Synchronizing Rock Clocks of Earth History. *Science* 320(5875):500–504
- Lourens LJ, Hilgen FJ, Laskar J, Shackleton NJ, Wilson D (2004) The Neogene Period. In: Gradstein FM, Ogg JG, Smith AG (eds) *Geologic Time Scale 2004*. Cambridge University Press, pp 409–440
- Lukács R, Harangi S, Bachmann O, Guillong M, Daniščík M, Buret Y, von Quadt A, Dunkl I, Fodor L, Sliwinski J, Soós I, Szepesi J (2015) Zircon geochronology and geochemistry to constrain the

- youngest eruption events and magma evolution of the Mid-Miocene ignimbrite flare-up in the Pannonian Basin, eastern central Europe. *Contributions Miner Petrol* 170:52
- Márton E, Pécskay Z (1998) Complex evaluation of paleomagnetic and K/Ar isotope data of the Miocene ignimbritic volcanics in the Bükk Foreland, Hungary. *Acta Geol Hung* 41:467–476
- Mattinson J (2005) Zircon U–Pb chemical abrasion (“CA-TIMS”) method: combined annealing and multi-step partial dissolution analysis for improved precision and accuracy of zircon ages. *Chem Geol* 220:47–66
- Min K, Mundil R, Renne PR, Ludwig KR (2000) A test for systematic errors in $^{40}\text{Ar}/^{39}\text{Ar}$ geochronology through comparison with U/Pb analysis of a 1.1-Ga rhyolite. *Geochim Cosmochim Acta* 64:73–98
- Morgan LE, Renne PR, Taylor RE, WoldeGabriel G (2009) Archaeological age constraints from eruption ages of obsidian: examples from the Middle Awash, Ethiopia. *Quat Geochron* 4:193–203
- Nagra (2008) Radiometrische Altersbestimmung an Bentonitproben der Oberen Süßwassermolasse (OSM), Zwischenbericht mit provisorischen Daten. Nagra int. Ber. NIB 08-07
- Pavoni N, Schindler C (1981) Bentonitvorkommen in der Oberen Süßwassermolasse des Kantons Zürich und damit zusammenhängende Probleme. *Eclog Geol Helvet* 74:53–64
- Pécskay Z, Lexa J, Szakás A, Seghedi I, Balogh K, Konečný V, Zelenka T, Kovacs M, Póka T, Fülöp A, Márton E, Panaiotu C, Cvetković V (2006) Geochronology of Neogene magmatism in the Carpathian arc and intra-Carpathian area. *Geol Carpathica Bratislava* 57:511–530
- Phillips D, Matchan E (2013) Ultra-high precision $^{40}\text{Ar}/^{39}\text{Ar}$ ages for Fish Canyon Tuff and Alder Creek Rhyolite sanidine: new dating standards required? *Geochim Cosmochim Acta* 121:229–239
- Pohl J (1965) Die Magnetisierung der Suevite des Rieses. *N Jb Miner Mh* 9–11:288–2766
- Pohl J (1977) Paläomagnetische und gesteinsmagnetische Untersuchungen an den Kernen der Forschungsbohrung Nördlingen 1973. *Geol Bavarica* 75:329–348
- Pohl J, Poschlod K, Reimold WU, Meyer C, Jacob J (2010) Ries Crater, Germany: the Enkingen magnetic anomaly and associated drill core SUBO 18. *Geol Soc Am Spec Pap* 465:141–163
- Prieto J, Böhme M, Maurer H, Heissig K, Aziz HA (2009) Sedimentology, biostratigraphy and environments of the Untere Fluviale Serie (Lower and Middle Miocene) in the central part of the North Alpine Foreland Basin—implications for basin evolution. *Int J Earth Sci* 98:1767–1791
- Reichenbacher B, Böttcher R, Bracher H, Doppler G, Von Engelhardt W, Gregor H-J, Heissig K, Heizmann EPJ, Hofmann F, Kälin D, Lemcke K, Luterbacher H, Martini E, Pfeil F, Reiff W, Schreiner A, Steininger FF (1998) Graupensandrinne-Ries-Impakt: Zur Stratigraphie der Grimmelfinger Schichten, Kirchberger Schichten und Oberen Süßwassermolasse (nördliche Vorlandmolasse, Süddeutschland). *Z deutsch geol Gesell* 149:127–161
- Reichenbacher B, Krijgsman W, Lataster Y, Pippèr M, Van Baak CGC, Chang L, Kälin D, Jost J, Doppler G, Jung D, Prieto J, Aziz HA, Böhme M, Garnish J, Kirscher U, Bachtadse V (2013) An alternative magnetostratigraphic framework for the Lower Miocene (Ottangian, Karpatian) in the North Alpine Foreland Basin. *Swiss J Geosci* 106:309–334
- Reid MR, Coath CD, Harrison TM, McKeegan KD (1997) Prolonged residence times for the youngest rhyolites associated with Long Valley Caldera: $^{230}\text{Th}/^{238}\text{U}$ microprobe dating of young zircons. *Earth Planet Sci Lett* 150:27–39
- Renne PR, Swisher CC, Deino AL, Karner DB, Owens TL, De Paolo DJ (1998) Intercalibration of standards, absolute ages and uncertainties in $^{40}\text{Ar}/^{39}\text{Ar}$ dating. *Chem Geol* 145:117–152
- Renne PR, Mundil R, Balco G, Min K, Ludwig KR (2010) Joint determination of ^{40}K decay constants and $^{40}\text{Ar}^*/^{40}\text{K}$ for the Fish Canyon sanidine standard, and improved accuracy for $^{40}\text{Ar}/^{39}\text{Ar}$ geochronology. *Geochim Cosmochim Acta* 74:5349–5367
- Renne PR, Balco G, Ludwig KR, Mundil R, Min K (2011) Response to the comment by W.H. Schwarz, on “Joint determination of ^{40}K decay constants and $^{40}\text{Ar}^*/^{40}\text{K}$ for the Fish Canyon sanidine standard, and improved accuracy for $^{40}\text{Ar}/^{39}\text{Ar}$ geochronology” by Renne et al. (2010). *Geochim Cosmochim Acta* 75:5097–5100
- Reuter L (1925) Die Verbreitung jurassischer Kalkblöcke aus dem Ries im südbayerischen Diluvialgebiet (Ein Beitrag zur Lösung des Riesproblems). *Jber Mitt oberh geol Ver* 14:191–218
- Rögl F (1998) Paleogeographic considerations for Mediterranean and Paratethys Seaways (Oligocene to Miocene). *Ann Naturhist Mus Wien* 99A:279–310
- Rummel M (2000) Die Cricetodontini aus dem Miozän von Petersbuch bei Eichstätt. *Die Gattung Cricetodon Lartet 1851*. *Senckenb Lethaea* 80:149–171
- Sawatzki G, Schreiner A (1991) Bentonit und Deckentuffe am Hohenstoffeln/Hegau. *Jh geol Landesamt Baden-Württemberg* 33:59–73
- Schaltegger U, Schmitt A, Horstwood M (2015) U–Th–Pb zircon geochronology by ID-TIMS, SIMS and laser ablation ICP-MS: recipes, interpretations and opportunities. *Chem Geol* 402:89–110
- Schärer U (1984) The effect of initial ^{230}Th disequilibrium on young U–Pb ages: the Makalu case, Himalaya. *Earth Planet Sci Lett* 67:191–204
- Scheuenpflug L (1980) Neue Funde ortsfremder Weißjuragesteine in Horizonten der südbayerischen miozänen Oberen Süßwassermolasse um Augsburg. *Jber Mitt oberh-geol Ver NF* 62:131–142
- Schlunegger F, Jordan TE, Klaper EM (1997) Controls of erosional denudation in the orogen on foreland basin evolution: the Oligocene central Swiss Molasse Basin as an example. *Tectonics* 16:823–840
- Schmid W (1995) Lithofazielle Untersuchungen im tertiären Hügelland nördlich von Dasing (Landkreis Aichach-Friedberg) einschließlich Erläuterungen zur geologischen Karte. Unpubl Dipl thesis, Ludwig-Maximilians-University, Munich
- Schmitz MD, Schoene B (2007) Derivation of isotope ratios, errors, and error correlations for U–Pb geochronology using Pb-205–U-235–(U-233)-spiked isotope dilution thermal ionization mass spectrometric data. *Geochem Geophys Geosyst* 8:Q08006
- Schoene B, Crowley J, Condon D, Schmitz M, Bowring S (2006) Reassessing the uranium decay constants for geochronology using ID-TIMS U–Pb data. *Geochim Cosmochim Acta* 70:426–445
- Schoene B, Schaltegger U, Brack P, Latkoczy C, Stracke A, Günther D, Samperton K (2012) Rates of magma differentiation and emplacement in a ballooning pluton recorded by U–Pb TIMS-TEA, Adamello batholith, Italy. *Earth Planet Sci Lett* 355–356:162–173
- Schreiner A (2008) Hegau und westlicher Bodensee. *Sammlung geologischer Führer*, vol 62, 3rd edn. Schweizerbart Sci Pub, Stuttgart
- Seghedi I, Downes H, Szakás A, Mason PRD, Thirwall MF, Rosu E, Pécskay Z, Márton E, Panaiotu C (2004) Neogene–quaternary magmatism and geodynamics in the Carpathian–Pannonian region: a synthesis. *Lithos* 72:117–146
- Steiger RH, Jäger E (1977) Subcommission on geochemistry: convention on the use of decay constants in geo- and cosmochronology. *Earth Planet Sci Lett* 36:359–362
- Stephan W (1952) Ein tortoner Brockhorizont in der Oberen Süßwassermolasse Bayerns. *Geol Bavarica* 14:6–85

- Szakács A, Zelenka T, Márton E, Pécskay Z, Póka T, Seghedi I (1998) Miocene acidic explosive volcanism in the Bükk Foreland, Hungary: identifying eruptive sequences and searching for source locations. *Acta Geol Hung* 41:413–435
- Szakács A, Vlad D, Andriessen PAM, Fülöp A, Pécskay Z (2000) Eruptions of the “Dej Tuff”: when, where and how many? *Vijesti Hrv. Geol. Društva* 37, 3, PANCARDI 2000 Spec. Issue, Abstract Vol. 1: 122
- Szakács A, Pécskay Z, Silye L, Balogh K, Vlad D, Fülöp A (2012) On the age of the Dej Tuff, Transylvanian Basin (Romania). *Geol Carpathica* 63:139–148
- Turco E, Hüsing S, Hilgen F, Cascella A, Gennari R, Iaccarino SM, Sagnotti L (2017) Astronomical tuning of the La Vedova section between 16.3 and 15.0 Ma. Implications for the origin of megabeds and the Langhian GSSP. *Newsl Stratigr* 50:1–29
- Ulbig A (1994) Vergleichende Untersuchungen an Bentoniten, Tuffen und sandig-tonigen Einschaltungen in den Bentonitlagerstätten der Oberen Süßwassermolasse Bayerns. Dissertation thesis, TUM, Munich, 245 p
- Ulbig A (1999) Untersuchungen zur Entstehung der Bentonite in der bayerischen Oberen Süßwassermolasse—Investigations on the origin of the bentonite deposits in the Bavarian Upper Freshwater Molasse. *N Jb Geol Paläont Abh* 214:497–508
- Unger HJ, Niemeyer A (1985a) Bentonitlagerstätten zwischen Mainburg und Landshut und ihre zeitliche Einstufung. *Geol Jb* D71:59–93
- Unger HJ, Niemeyer A (1985b) Bentonite in Ostniederbayern—Entstehung, Lagerung, Verbreitung. *Geol Jb* D71:3–58
- Unger HJ, Fiest W, Niemeyer A (1990) Die Bentonite der ostbayerischen Molasse und ihre Beziehung zu den Vulkaniten des Panonischen Beckens. *Geol Jb* D96:67–112
- Viertel C (1995) Palynologisch stratigraphische Untersuchungen Miozäner Kohlen und Tone der Grube Rohrhof II bei Pohnholz/Oberpfalz. Doctoral Dissertation, Ludwig Maximilians University Munich
- Villa IM (1997) Direct determination of ^{39}Ar recoil distance. *Geochim Cosmochim Acta* 61(3):689–691
- Vogt K (1980) Bentonite deposits in Lower Bavaria. *Geol Jb* D39:47–68
- Wappenschmidt I (1936) Zur Geologie der Oberpfälzer Braunkohle. *Abh Geol Landesuntersuchung am Bayer Oberbergamt* 25:1–68
- Wendt I, Carl C (1991) The statistical distribution of the mean squared weighted deviation. *Chem Geol Isot Geosci Sect* 86:275–285
- Wotzlaw JF, Schaltegger U, Frick DA, Dungan MA, Gerdes A, Günther D (2013) Tracking the evolution of large volume silicic magma reservoirs from assembly to supereruption. *Geology* 41:867–870
- Wotzlaw JF, Bindeman IN, Watts KE, Schmitt AK, Caricchi L, Schaltegger U (2014a) Linking rapid magma reservoir assembly and eruption trigger mechanisms at evolved Yellowstone-type supervolcanoes. *Geology* 42:807–810
- Wotzlaw JF, Hüsing SK, Hilgen FJ, Schaltegger U (2014b) High-precision U–Pb geochronology of astronomically dated volcanic ash beds from the Mediterranean Miocene. *Earth Planet Sci Lett* 407:19–34
- Zeeden C, Rivera TA, Storey M (2014) An astronomical age for the Bishop Tuff and concordance with radioisotopic dates. *Geophys Res Lett* 41:3478–3484